Functional interplay between protein acylation and cellular metabolism in metabolic disorders

Pougovkina, O.A.

Chapter 4

Proteomic and biochemical studies of lysine malonylation suggests its malonic aciduria-associated regulatory role in mitochondrial function and fatty acid oxidation

Gozde Colak[1], Olga Pougovkina[2], Lunzhi Dai[1], Minjia Tan[3], Heleen te Brinke[2], He Huang[1], Zhongyi Cheng[4], Jeongsoon Park[5], Xuelian Wan[3], Xiaojing Liu[6], Wyatt W. Yue[7], Ronald J. A. Wanders[2,8], Jason W. Locasale[6], David B. Lombard[5], Vincent C. J. de Boer[2,8*], and Yingming Zhao[1,3]

Mol Cell Proteomics. 2015 Aug 28.

Proteomic and biochemical studies of lysine malonylation suggests its malonic aciduria-associated regulatory role in mitochondrial function and fatty acid oxidation

Gozde Colak[1], Olga Pougovkina[2], Lunzhi Dai[1], Minjia Tan[3], Heleen te Brinke[2], He Huang[1], Zhongyi Cheng[4], Jeongsoon Park[5], Xuelian Wan[3], Xiaojing Liu[6], Wyatt W. Yue[7], Ronald J. A. Wanders[2,8], Jason W. Locasale[6], David B. Lombard[5], Vincent C. J. de Boer[2,8*], and Yingming Zhao[1,3]

Mol Cell Proteomics. 2015 Aug 28.

[1]Ben May Department of Cancer Research, University of Chicago, Chicago, IL, 60637, USA
[2]Laboratory Genetic Metabolic Diseases, Department of Clinical Chemistry, Academic Medical Center, University of Amsterdam, Meibergdreef 9, 1105 AZ, Amsterdam, The Netherlands
[3]State Key Laboratory of Drug Research, Shanghai Institute of Materia Medica, Chinese Academy of Sciences, Shanghai, 201203, P.R. China
[4]PTM Biolabs, Chicago, IL 60612, USA
[5]Department of Pathology and Institute of Gerontology, University of Michigan, Ann Arbor, MI 48109, USA
[6]Division of Nutritional Sciences, Cornell University, Ithaca, NY 14853
[7]Structural Genomics Consortium, University of Oxford, Oxford OX3 7DQ, UK
[8]Department of Pediatrics, Emma's Children Hospital, Academic Medical Center, University of Amsterdam, Meibergdreef 9, 1105 AZ Amsterdam, The Netherlands

Abstract

The protein substrates of SIRT5-regulated lysine malonylation (Kmal) remain unknown, hindering its functional analysis. In this report, we carried out proteomic screening, identifying 4042 Kmal sites on 1426 proteins in mouse liver, and 4943 Kmal sites on 1822 proteins in human fibroblasts. Elevated malonyl-CoA in Malonyl-CoA decarboxylase (MCD) deficient cells induces Kmal levels in substrate proteins. We identified 461 Kmal sites showing more than 2-fold increase in response to MCD deficiency, as well as 1452 Kmal sites detected only in $MCD^{-/-}$ fibroblast but not in $MCD^{+/+}$ cells, suggesting a pathogenic role of Kmal in MCD deficiency. Lysine malonylation impaired mitochondrial function and fatty acid oxidation in MCD deficient cells, indicating that lysine malonylation could contribute to the pathophysiology of malonic aciduria. Our study establishes an association between Kmal and a genetic disease, and offers a rich resource for elucidating the contribution of the Kmal pathway and malonyl-CoA to cellular physiology and human diseases.

Introduction

Reversible acetylation at lysine residues in proteins has been extensively studied over the past few decades (Roth et al., 2001; Yang and Seto, 2007). This modification is now known to have important regulatory roles in diverse cellular processes and physiological conditions, such as transcription, metabolism, and aging (Chang and Guarente, 2014; Giblin et al., 2014; Wagner and Hirschey, 2014). Dysregulation of the lysine acetylation pathway is associated with various diseases, such as cardiovascular disease and cancer (Haberland et al., 2009; Lee et al., 2012). In addition to acetylation, recent studies show that lysine residues in proteins can be modified by a family of short-chain acylations: propionylation, butyrylation, crotonylation, malonylation, succinylation, glutarylation, and 2-hydroxyisobutyrylation (Dai et al., 2014; Du et al., 2011; Park et al., 2013; Tan et al., 2011; Tan et al., 2014; Xie et al., 2012). Notable among the seven types of new lysine acylation pathways are lysine malonylation (Kmal), succinylation (Ksucc), and glutarylation (Kglu). Each of the three types of modifications have an acidic carboxylic group that changes the charge status from +1 to -1 charge at physiological pH, which is similar to that caused by protein phosphorylation, but more significant than lysine acetylation (Fig. 1A). Accordingly, these acidic lysine acylations are likely to have a more substantial impact on the substrate protein's structure and function than lysine acetylation, when modified at the same lysine residue(s). Recent studies demonstrate that pyruvate dehydrogenase complex (PDC), succinate dehydrogenase, and carbamoyl phosphatase synthase 1 (CPS1) can be regulated by Ksucc and Kglu, respectively, suggesting that acidic lysine acylation pathways can have unique functions distinct from the widely studied lysine acetylation pathway (Park et al., 2013; Tan et al., 2014).

Kmal was initially identified in both *E. coli* and mammalian cells by using HPLC-MS/MS, co-elution of synthetic peptides, isotopic labeling, and Western blotting analysis with pan α-Kmal antibodies (Peng et al., 2011a; Xie et al., 2012). The Lin group and our group have previously demonstrated robust enzymatic activities of SIRT5, both *in vitro* and *in vivo*, in demalonylation, desuccinylation and deglutarylation (Peng et al., 2011a). The demalonylation and desuccinylation activities of SIRT5 require NAD^+, but can be inhibited by nicotinamide, a class III HDAC inhibitor. Given the fact that isotopic malonate can label lysine malonylation and that acyl-CoAs are the precursor for other lysine acylations (e. g., acetyl-CoA for lysine acetylation), malonyl-CoA is likely to be the precursor for the lysine malonylation reaction (Peng et al., 2011a; Xie et al., 2012). Despite the progress, the substrates for this new modification pathway remain largely unknown, representing a major bottleneck for studying its biological functions.

Malonyl-CoA is a tightly regulated metabolic intermediate in mammalian cells (Saggerson, 2008). Malonyl-CoA is produced by acetyl-CoA carboxylase and consumed by malonyl-CoA decarboxylase (MCD, E.C. 4.1.1.9), fatty acid synthase (FAS), and fatty acid elongases (Saggerson, 2008) (Fig. 1B). In addition to being a key intermediate for fatty acid biosynthesis and fatty acid elongation, malonyl-CoA has diverse regulatory functions. Malonyl-CoA was shown to be a potent inhibitor of carnitine palmitoyl transferase 1 (CPT1) regulating hepatic fatty acid

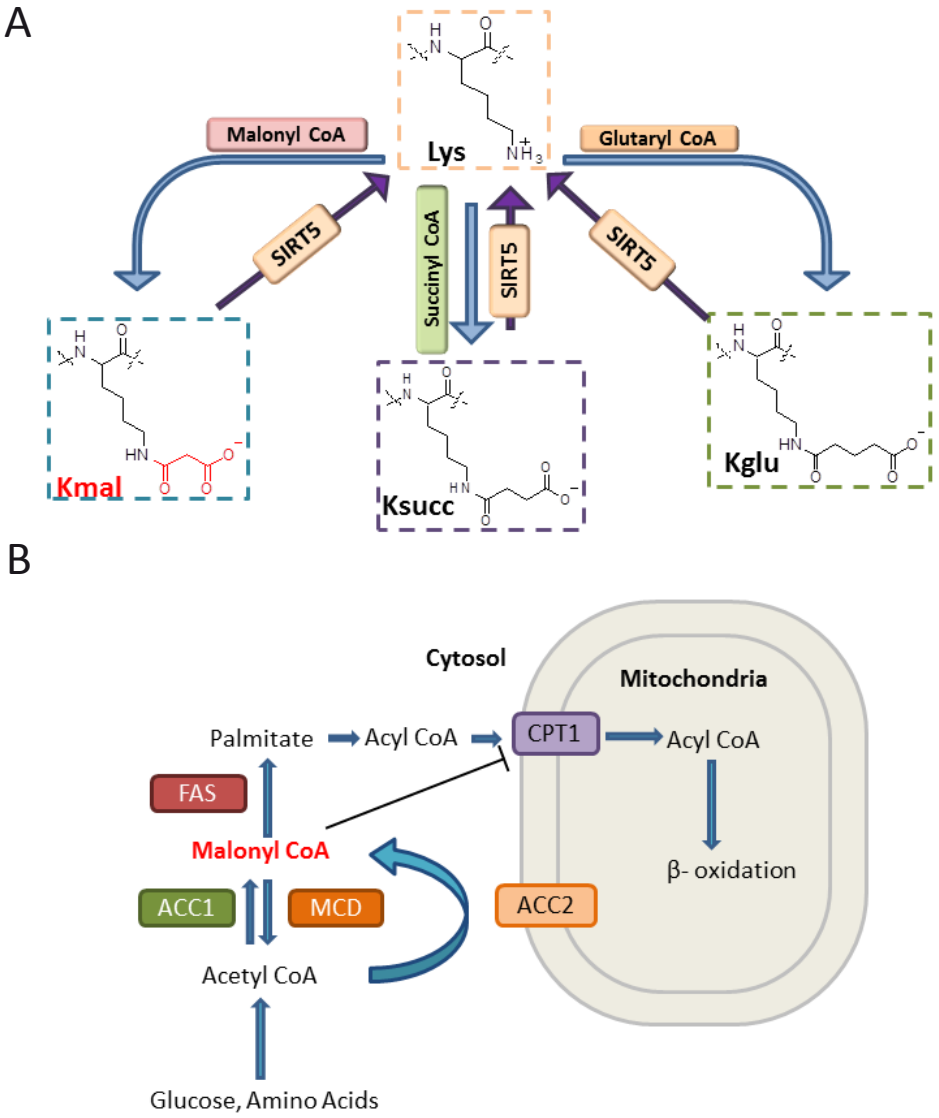

Figure 1. Lysine malonylation and biosynthesis of malonyl-CoA. (A) Structures of malonyllysine (Kmal), succinyl-lysine (Ksucc) and glutaryllysine (Kglu). SIRT5 is an enzyme with demalonylation, desuccinylation and deglutarylation activities. (B) Illustration of malonyl-CoA metabolism with FAS (fatty acid synthase), ACC1 and ACC2 (acetyl-CoA carboxylase1 and 2), MCD (malonyl-CoA decarboxylase), CPT1 (carnitine palmitoyl transferase 1).

synthesis, β-oxidation, and ketogenesis (Saggerson, 2008) (Fig. 1B). It was reported that malonyl-CoA can function as a key intermediate in the hypothalamus as an energy sensor (Wolfgang and Lane, 2008). Higher malonyl-CoA levels are observed in skeletal muscle biopsies of type 2 diabetic patients (Bandyopadhyay et al., 2006). Elevated fatty acid oxidation observed during cardiac ischemia/reperfusion has been attributed to the reduction of malonyl-CoA levels in the heart. Accordingly,

increasing malonyl-CoA levels has been proposed as a strategy to improve cardiac function (Fillmore and Lopaschuk, 2014). Acetyl-CoA carboxylases, enzymes that are known to be important for biosynthesis of malonyl-CoA, are associated with various metabolic disorders. Mice with genetic knockout of acetyl-CoA carboxylase 2 gene are resistant to obesity and diabetes, when fed with high calorie diets (Abu-Elheiga et al., 2003). Accordingly, acetyl-CoA carboxylases have been proposed as drug targets for diverse human diseases, including diabetes, obesity, and cancer (Tong and Harwood, 2006). Nevertheless, potential roles for malonyl-CoA in human pathology are not well understood.

MCD is a 55 kDa enzyme that catalyzes conversion of malonyl-CoA to acetyl-CoA, thus maintaining homeostatic levels of these metabolites in mitochondria and peroxisomes. In the cytosol, malonyl-CoA is controlled by two enzymes with opposing activities, MCD and acetyl-CoA carboxylase. MCD deficiency, or malonic aciduria, is an inborn metabolic disorder caused by MCD mutations that reduce or eliminate activity of this enzyme and therefore compromise the conversion of malonyl-CoA to acetyl-CoA (FitzPatrick et al., 1999). These patients have high levels of malonylcarnitine (C3DC) in blood and high level of organic acids, such as malonic acid, in the urine (Santer et al., 2003). Diverse symptoms are observed among the malonic aciduria patients, including delayed development, seizures, diarrhea, vomiting, low blood sugar (hypoglycemia) and cardiomyopathy (FitzPatrick et al., 1999). It appears that inhibition of fatty acid catabolism caused by high level of malonyl-CoA is at least partially responsible for the manifestations of disease. We recently showed that MCD deficient patient cells ($MCD^{-/-}$) show increased Kmal levels (Pougovkina et al., 2014). It is therefore possible that Kmal could be an important mechanism mediating the pathophysiology of MCD deficiency. Nevertheless, how the increased Kmal levels, caused by high level of malonic acid in malonic aciduria patients and in other diseases, impact cellular function and regulate physiology remains unknown.

In this study, we used a proteomic approach to identify Kmal substrates and map their modification sites, by affinity enrichment of malonylated peptides and HPLC-MS/MS analysis. We identified 4016 Kmal sites on 1395 proteins in SIRT5 knockout mouse liver, and 4943 Kmal peptides on 1831 proteins in $MCD^{+/+}$ and $MCD^{-/-}$ human fibroblasts. 461 Kmal sites on 339 proteins showed a 2-fold increase or more in $MCD^{-/-}$ cells relative to $MCD^{+/+}$ cells, and 1452 Kmal sites on 822 proteins were only detected in $MCD^{-/-}$ cells, suggesting that MCD activity has a profound impact on Kmal levels and distribution. The malonylated proteins indentified in $MCD^{-/-}$ cells are associated with diverse pathways, including fatty acid metabolism and neurological diseases. We further showed that lysine malonylation inhibits mitochondrial respiration and impacts fatty acid oxidation in $MCD^{-/-}$ cells. Our proteomics data illuminates the landscape of the Kmal modification in mammalian cells, offering a valuable resource for studying its biology, and providing key insights into the role of Kmal in diseases associated with dysregulation of malonyl-CoA homeostasis.

Materials and methods

Materials

Chemicals were purchased as analytical grade from Sigma-Aldrich, Inc. (St. Louis, MO). Modified sequencing-grade trypsin was purchased from Promega Corporation (Madison, WI). Pan α-malonyllysine antibody and pan α-malonyllysine agarose beads were from PTM Biolabs, Inc (Chicago, IL). MS grade water and acetonitrile were from Thermo Fisher Scientific (Waltham, MA). C18 ZipTips were purchased from Millipore Corporation (Billerica, MA). SILAC DMEM media (CCFDA003-132J01) was purchased from UCSF Cell Culture Facility (San Francisco, CA). XerumFree reagent (XF205) was purchased from MayFlower Bioscience (St. Louis, MO). Dialyzed serum (Gibco-26400) was purchased from Life Technologies, Thermo Fisher Scientific (Grand Island, NY).

Preparation of mouse liver lysate

Four two-month old male SIRT5 KO mice (Lombard et al., 2007; Nakagawa et al., 2009) were anesthetized with isoflurane overdose, and the blood in the liver was removed by perfusion with ice-cold PBS for 5 min. Liver was homogenized in a glass dounce homogenizer in SDS lysis buffer (20 mM Tris-Cl pH 6.8, 1% SDS, 5% β-Mercaptoethanol, 10% glycerol, 25 mM nicotinamide). The lysates from four livers were pooled together and the sample was clarified by centrifugation at 16,000 g. The protein in the supernatant was precipitated with 10% (v/v) trichloroacetic acid. Then the precipitated proteins were in-solution digested with trypsin as previously described (Kim et al., 2006a).

Preparation of SILAC samples

Human dermal fibroblast cells lines: $MCD^{+/+}$ (control cells) and $MCD^{-/-}$ (malonyl-CoA decarboxylase deficient cells) were obtained from Gaslini BioBank, Italy. The cells were grown in SILAC DMEM, supplemented with L-Glutamine (584 mg/L), 10% (v/v) dialyzed serum, and 2% (v/v) Serum Free reagent. Regular L-Lysine ($^{12}C_6{}^{14}N_2$) and L-Arginine ($^{12}C_6{}^{14}N_2$) were added to the "Light" media (final concentration: 100 mg/L) used for culturing $MCD^{-/-}$ cells. "Heavy" isotopic L-Lysine ($^{13}C_6{}^{15}N_2$) and "light" L-Arginine ($^{12}C_6{}^{14}N_2$) was added to the "Heavy" media (final concentration: 100 mg/L) used for culturing $MCD^{+/+}$ control cells. Both cells were grown in parallel, until $MCD^{+/+}$ cells were sufficiently labeled by the isotopic lysine. Both $MCD^{+/+}$ and $MCD^{-/-}$ cells were lysed in SDS buffer (20 mM Tris-HCl pH 6.8, 1% SDS, 5% β-Mercaptoethanol, 10% glycerol, 25 mM nicotinamide). Twelve milligram of each cell lysate were mixed and then precipitated overnight by 10% TCA for tryptic digestion.

HPLC Fractionation

The tryptic peptides were fractionated by using a reversed-phase column (Luna C18 10 mm x 250 mm, 5 μm particle, 100 Å pore size, Phenomenex Inc., Torrance, CA) in Discovery VP preparative HPLC system (Shimadzu Corp., Kyoto, Japan). The peptides were fractionated into 75 fractions using a gradient from 2% to 90% buffer B (10 mM ammonium formate in 90% acetonitrile and 10% water, pH 7.8) in buffer A

(10 mM ammonium formate in water, pH 7.8) at a flow rate of 4 ml/min in 60 min. The 75 fractions were finally combined equally into 5 final fractions for mouse liver samples, and 10 final fractions for MCD SILAC sample, respectively. Each fraction was condensed by using SpeedVac (ThermoSavant SPD111V). The peptide solution was then used for immunoaffinity enrichment. Affinity Enrichment of the Peptides Containing Kmal — The peptides containing Kmal were enriched using a procedure described previously (Kim et al., 2006a). The tryptic peptides from each fraction were resolubilized in 100 mM NH_4HCO_3 (pH 8.0). Samples were centrifuged at 20,000 g for 10 min to remove insoluble particles. The peptides were incubated with 15 µL of agarose beads conjugated with anti-malonyl lysine antibody at room temperature for 4 h with gentle rotation. The beads were washed three times with NETN buffer, twice with ETN buffer (50 mM Tris-HCl, pH 8.0, 100 mM NaCl, 1 mM EDTA) and once with water. Enriched Kmal peptides were eluted from the beads by washing three times with 0.1% trifluoroacetic acid. The eluted Kmal peptides were dried in a SpeedVac.

Nano-HPLC-MS/MS Analysis

The enriched Kmal samples were first desalted using OMIX C18 tips (Agilent Technologies Inc., Santa Clara, CA) and then dissolved in solvent A (0.1% formic acid in water). Samples were then injected onto a manually packed reversed-phase C18 column (100 mm × 75 µm, 3-µm particle size, Dr. Maisch GmbH, Ammerbuch, Germany) connected to an Easy-nLC 1000 HPLC system (Thermo Fisher scientific Inc., Waltham, MA). Peptides were eluted from 5% to 90% solvent B (0.1% formic acid and 1% water in acetonitrile) in solvent A with a 1 h gradient at a flow rate of 200 nl/min. The analytes were directly ionized and sprayed into a Q Exactive mass spectrometer (Thermo Fisher scientific Inc., Waltham, MA) by a Nanospray Flex™ Ion Sources. Full MS scans were acquired in the Orbitrap mass analyzer over the range m/z 300-1400 with a mass resolution of 70,000 at m/z 200. The 15 most intense peaks of the precursor ions were fragmented in the HCD collision cell with normalized collision energy of 27, and tandem mass spectra were acquired with a mass resolution of 17,500 at m/z 200. Lock mass at m/z 445.120024 was enabled for internal calibration of full MS spectrum. Ions with either a single charge or more than 4 charges were excluded from MS/MS fragmentation and the dynamic exclusion duration was set to 25s.

Data Processing and Analysis

MaxQuant software (v 1.3.0.5) was used for identifying and quantifying protein and malonylated peptides. Peaklist generation and precursor mass recalibration of the raw MS data were carried out by MaxQuant software. Trypsin was specified as the cleavage enzyme and the maximum number of missed cleavage was set at 3. Methionine oxidation, protein N-terminal acetylation, lysine acetylation (Kac), Kmal (specified for neutral loss of CO_2 in MS/MS fragmentation), and Ksucc were specified as variable modifications, and cysteine alkylation by iodoacetamide was specified as a fixed modification for all database searching. Database searching was performed against the UniProt mouse (50,807 sequences) or human (88,817

sequences) reference protein sequence database concatenated with reversed decoy database with initial precursor mass tolerance of 7 ppm. Mass tolerance for fragment ions was set at 20 ppm. False discovery rate (FDR) thresholds for protein, peptide and modification site were fixed at 0.01. The identified peptides with MaxQuant Andromeda score below 50 and localization probability below 0.75 were further removed prior to bioinformatics analysis.

Malonyl-CoA Measurement

The cells were treated with 15 µM Orlistat or vehicle only for 24 h at 80% confluence. The media were quickly removed and the dish was placed on top of dry ice. One ml of extraction solvent (80% methanol/water) was immediately added, and the dishes were then transferred to the -80°C freezer. The dishes were left for 15 min and then cells were scraped into extraction solvent on dry ice. The whole solution was centrifuged with the speed of 20,000 g at 4°C for 10 min. Here, cell extracts were prepared from three wells to make biological triplicates. The supernatant from tissue extract was transferred to a new tube for LC-QE-MS analysis. All samples were dried in a vacuum concentrator (Speed Vac). Ultimate 3000 UHPLC (Dionex) was coupled to Q Exactive-Mass spectrometer (QE-MS, Thermo Scientific) for metabolite separation and detection. For Acyl-Coenzyme A (Acyl-coA) analysis, a reversed phase liquid chromatography (RPLC) method was used. A Luna C18 column (100 x 2.0 mm i.d., 3 µm; Phenomenex) was employed with mobile phase A: water with 5 mM ammonium acetate (pH = 6.8), and mobile phase B: methanol, at a flow rate of 0.2 ml/min. The linear gradient was: 0 min, 2% B; 1.5 min, 2% B; 3 min, 15% B; 5.5 min, 95% B; 14.5 min, 95% B; 15 min, 2% B, 20 min, 2% B. The column was at room temperature. The Q Exactive mass spectrometer (QE-MS) was equipped with a HESI probe, and the relevant parameters were as follows: heater temperature, 120°C; sheath gas, 30; auxiliary gas, 10; sweep gas, 3; spray voltage, 3.6 kV for positive mode. The capillary temperature was set at 320°C, and S-lens was 55. A full scan range was set at 300 to 1000 (m/z). The resolution was set at 70 000 (at m/z 200). The maximum injection time (max IT) was 200 ms. Automated gain control (AGC) was targeted at 3 × 106 ions. For CoA analysis, cell extract was dissolved into 30 µl of water with 50 mM ammonium acetate, pH 6.8. Samples were centrifuged at 20,000 g at 4°C for 3 min and the supernatant was transferred to LC vials. The injection volume was 8 µl for CoA analysis. Raw data collected from LC-QE-MS were processed on Thermo Scientific software Sieve 2.0. Peak alignment and detection were performed according to manufacturer's protocols. For a targeted metabolomics analysis, a frameseed including Acyl-CoA metabolites that has been previously validated was used for targeted metabolite analysis with data collected in positive mode, with the m/z width set at 8 ppm. Statistical significance was calculated based on student's t test (unpaired, two tailed).

Motif Analysis for Lysine Malonylation Substrates

The standalone version of iceLogo (version 1.2) software was used to analyze the preference of flanking Kmal site sequence from mouse liver or human MCD cells (Colaert et al., 2009). The embedded Swiss-Prot "*Mus musculus*" or "*Homo sapiens*"

was used as the negative set. Six flanking amino acid residues on each side of a lysine malonylated site were selected as the positive set.

Functional Enrichment Analysis

Functional enrichment analysis of lysine malonylated proteins was carried out using DAVID (Functional Annotation Bioinformatics Microarray Analysis) Bioinformatics Resources v 6.7 with the total mouse or human genome information as the background (Huang da et al., 2009). All identified lysine malonylated proteins were subjected to database analyses using Gene Ontology (GO) (Ashburner et al., 2000) and Kyoto Encyclopedia of Genes and Genomes (KEGG) metabolic pathways (Kanehisa and Goto, 2000). GO FAT database from DAVID was selected in this analysis. The family-wide false discovery rate was corrected by Benjamini-Hochberg method using adjusted P value cutoff 0.05.

Protein-Protein Interaction Network Analysis

Protein-protein interaction networks of lysine malonylome were analyzed using STRING (Search Tool for the Retrieval of Interacting Genes/Proteins) database (version 9.1, confidence score 0.7) visualized by Cytoscape software (version 3.1.0) with MCODE App toolkit (Jensen et al., 2009). The confidence score is the approximate probability that a predicted link exists between two enzymes in the same metabolic map in the KEGG database. Confidence limits are as follows: low confidence 0.2 (or better), medium confidence 0.5, high confidence 0.75, the highest confidence 0.95.

Protein complex enrichment analysis

Manually-curated core complexes indexed by CORUM (the comprehensive resource of mammalian protein complexes) database were used for the analysis of lysine malonylated substrates (http://mips.helmholtz-muenchen.de/genre/proj/corum). Mouse or human complexes indexed in the database were used for enrichment analysis of mouse liver or MCD human cells by Fisher's exact test. Complexes with adjusted p-value < 0.01 were considered as significant.

Kmal stoichiometry calculation

Absolute stoichiometry calculation of malonylated site in SILAC samples was based on the previously reported algorithm (Olsen et al., 2010) with slight modification (Colak et al., 2013). The calculation was based on the MS quantification data (SILAC ratio) of the Kmal peptides (x), the corresponding protein (z), and the corresponding unmodified peptide (y), with the assumption that only one type of PTM occurs at a given site. The SILAC ratios of unmodified peptides (y) and proteins (z) were calculated from the global protein expression analysis using the whole cell lysate mixture of SILAC labeled $MCD^{+/+}$ and $MCD^{-/-}$ cells without antibody affinity enrichment. For the calculation it was assumed that only one type of PTM occurred at the given site of interest. The unmodified peptide was defined as the longest completely digested part of the peptide sequence derived from the malonylated peptide, which contains no other PTM. The absolute stoichiometry was calculated based on the SILAC ratios

of x, y, and z using the same formula as previously reported (Olsen et al., 2010).

Mitochondrial respiratory flux analysis

Measurements of cellular oxygen consumption were performed using an extracellular flux analyzer (Seahorse BioScience, Billerica, U.S.A.). Fao hepatoma cells were incubated for 24 hours in culture medium (DMEM supplemented with 2 mM HEPES, 2% Pen/Strep and 10% FBS) containing 50 mM malonate. Next, cells were plated at 20,000 cells/well in Seahorse 96 well culture plates followed by overnight incubation in malonate-free medium. Human fibroblasts were maintained and plated in DMEM supplemented with 2 mM HEPES, 2% Pen/Strep and 10% FBS at 30.000 cells/well. Seahorse mitochondrial function analysis was performed using the digitonin cell permeabilization protocol (Salabei et al., 2014). Prior to measurements of respiration, culture medium was replaced with MAS buffer (pH, 7.4, 220 mM mannitol, 70 mM sucrose, 10 mM KH_2PO_4, 5 mM $MgCl_2$, 2 mM HEPES, 1 mM EGTA and 0.6% BSA-fatty acid free). Oxygen consumption rate (OCR) was analyzed following a single injection of either pyruvate/malate/ADP/digitonin, succinate/rotenone/ADP/digitonin or octanoylcarnitine/malate/ADP/digitonin, dissolved in MAS buffer without BSA at pH 7.4. Final digitonin concentration was 30 µg/ml for Fao hepatoma cells and 100 µg/ml for fibroblasts. Final substrate concentrations were: pyruvate (5 mM), malate (2.5 mM), succinate (10 mM), octanoylcarnitine (100 µM), ADP (1 mM). After injection of substrate, oligomycin was injected at 1.5 µM final concentration followed by injection of antimycin (2.5 µM) and rotenone (1.25 µM).

Very-long chain acyl-CoA dehydrogenase (VLCAD) activity analysis

VLCAD activity was analyzed by monitoring the specific conversion of palmitoyl-CoA (C16:0-CoA) into palmitenoyl-CoA (C16:1-CoA) in cell lysates (Nouws et al., 2010). Cell lysates (0.1 mg/ml) were incubated in 0.125 mM Tris pH 8.0 with 0.4 mM ferrocenium and 0.25 mM palmitoyl-CoA for 10 minutes at 37°C and the reaction was stopped by the addition of 10 µl 2N HCl followed by neutralization with 10 µl 2M KOH/0.6M MES. Samples were deproteinated with acetonitrile followed by separation of substrate and products on a reversed-phase C18 HPLC and UV detection.

Long-chain 3-hydroxy-acyl-CoA dehydrogenase (LCHAD) activity analysis

LCHAD activity was analyzed by incubating cell lysates (0.1 mg/ml) with 3-ketopalmitoyl-CoA (0.26 mM, synthesized in house) and NADH 0.4 mM in MES/KPi (100mM/200mM) buffer with 0.1% Triton (pH 6.2) for 5 minutes at 37°C using a procedure previously described (Wanders et al., 1990). To control for the conversion of 3-ketopalmitoyl-CoA by short-chain 3-hydroxy-acyl-CoA dehydrogenase (SCHAD), samples were incubated with and without N-Ethyl-Maleimide (NEM), because NEM inhibits only LCHAD and not SCHAD. After incubation, reactions were stopped with 10 µl 2N HCL followed by neutralization with 10 µl 2M KOH/0.6M MES. Samples were deproteinated with acetonitrile followed by separation of substrate and products on a reversed-phase C18 HPLC and UV detection.

Immunocytochemistry

MCD$^{+/+}$ and MCD$^{-/-}$ cells were grown on coverslips and treated with 15 μM orlistat for 48 hr. Mito-tracker red was added to the culture medium at 0.1 μM final concentration and incubated for 30 min. The cells were washed with PBS twice and fixed with 4% (v/v) paraformaldehyde and permeabilized with 0.2% (v/v) Triton-X. The cells were blocked with 2% bovine serum albumin for 2 hrs and incubated with the corresponding primary antibodies at 1.5 μg/ml final concentration overnight. The cells were washed with PBS twice and incubated with secondary antibody Alexa Fluor 488 (Invitrogen, Grand Island, NY) for 2 hrs, and washed with PBS twice. Hoechst (BD Biosciences, San Jose, CA) is added at 2 μg/ml final concentration and incubated for 15 min. The coverslips are washed with PBS twice and mounted. The imaging was performed by using Leica SP2 DMIRE2 confocal microscope, with HCX PL APO Ibd.BL 63X 1.4 oil objective.

Results

Kmal is affected by SIRT5 and MCD

Our previous studies showed that SIRT5 can catalyze the removal of malonyl groups from malonylated lysine residues, both *in vitro* and *in vivo* (Peng et al., 2011a). In addition, exogenous malonate can boost lysine malonylation, possibly by increasing intracellular concentrations of malonyl-CoA catalyzed by a short-chain acyl-CoA synthase (Peng et al., 2011a). Consistent with this result, SIRT5 KO mice showed increased Kmal and Ksucc levels compared to their wild-type counterparts, but not Kac (Fig. 2A).

We previously showed, by western blotting analysis, that Kmal levels are higher in MCD$^{-/-}$ cells than in MCD$^{+/+}$ cells (Pougovkina et al., 2014). This result, in combination with our earlier observation that malonate can enhance Kmal (Peng et al., 2011a), supports the hypothesis that MCD deficiency induces malonyl-CoA concentration that can in turn boost Kmal. If this is true, a reduction of lipid biosynthesis by reduced activity of fatty acid synthase (FAS) may also increase malonyl-CoA and Kmal levels. To test this, we treated both control MCD$^{+/+}$ and MCD$^{-/-}$ cells with orlistat, an inhibitor of fatty acid synthase (Kridel et al., 2004). Consistent with our hypothesis, we observed an increase of Kmal levels in response to orlistat in MCD$^{+/+}$ cells (Fig. 2B). In addition, orlistat further increased Kmal levels in MCD$^{-/-}$ cells compared to MCD$^{+/+}$ cells, while Kac and Ksucc levels remained largely unchanged (Fig. 2C).

To test whether the enhanced Kmal levels are correlated with higher amounts of malonyl-CoA, we measured intracellular malonyl-CoA levels in MCD$^{+/+}$ and MCD$^{-/-}$ cells using HPLC/MS-based metabolomics method. Our data showed that orlistat significantly increased intracellular malonyl-CoA levels in both cell lines (Fig. 2D), suggesting that increased lysine malonylation induced via orlistat treatment might be due to enhanced concentration of malonyl-CoA.

Taken together, three different strategies for enhancing malonyl-CoA levels lead to increased levels of lysine malonylation. This result is consistent with our previous work showing that increasing crotonyl-CoA, succinyl-CoA and glutaryl-CoA levels all result in increases of their respective lysine acylations (Tan et al., 2011; Tan et al.,

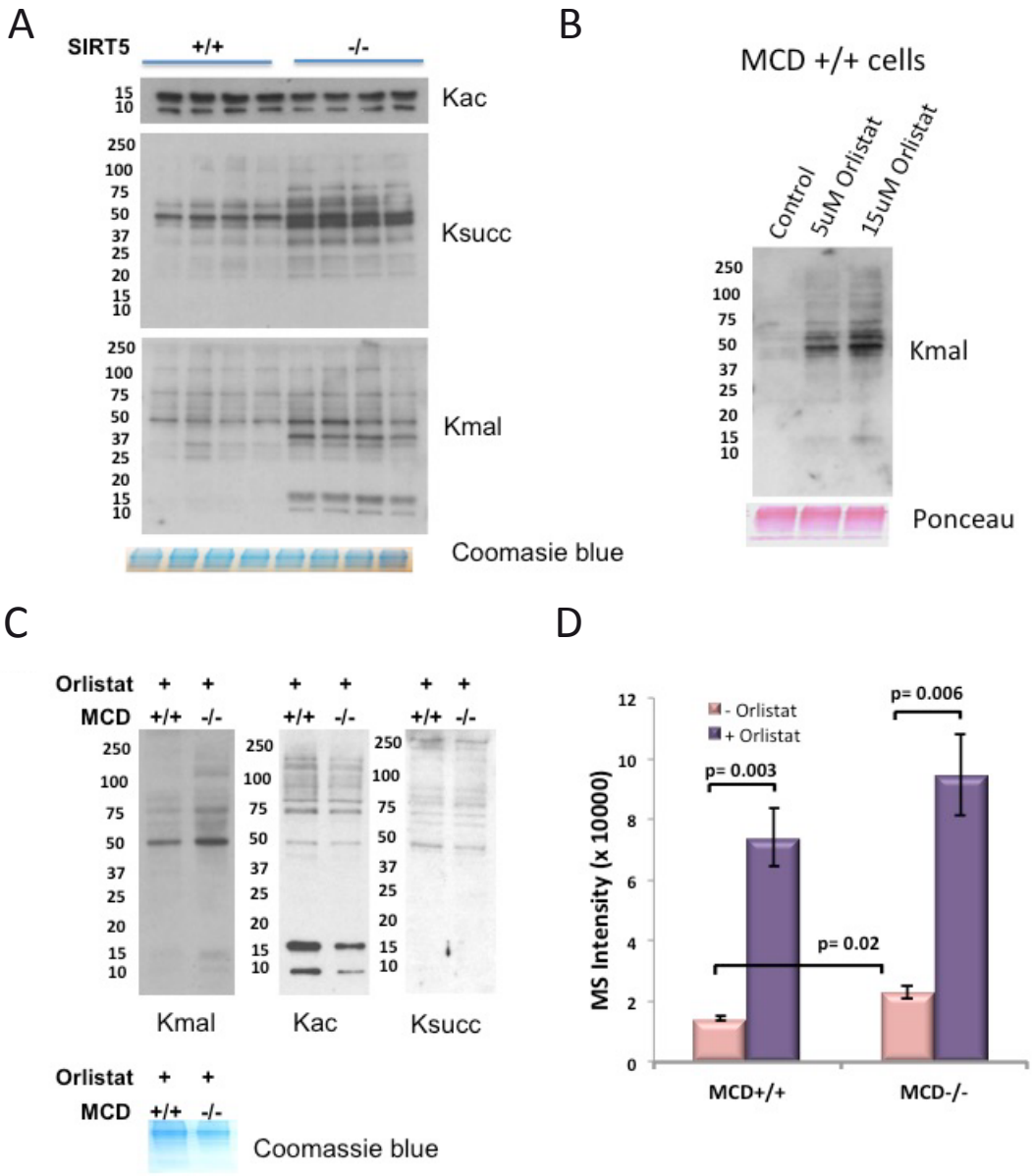

Figure 2. Dynamic changes of lysine malonylation vs other lysine acylations. (A) Lysine acylation levels in hepatocytes from (SIRT5$^{+/+}$) and SIRT5 knockout (SIRT5$^{-/-}$) mouse. Four pairs of mice were used. From top panel to bottom: α-acetyllysine blot, α-succinyllysine blot, α-malonyllysine blot, and Coomassie blue loading control. B) MCD$^{+/+}$ cells treated with 5 μM and 15 μM Orlistat for 48 h. Top: α-malonyllysine blot, bottom: ponceau loading control. (C) Dynamics of lysine acylation in response to orlistat, a FAS inhibitor. The MCD$^{+/+}$ and MCD$^{-/-}$ cells were both treated with 15 μM orlistat for 48 h. From left to right: α-malonyllysine blot, α-acetyllysine blot, α-succinyllysine blot, and Coomassie blue loading control. (D) Relative malonyl-CoA levels of MCD$^{+/+}$ and MCD$^{-/-}$ cells, with and without 24 h orlistat treatment. See also Fig. S1.

2014; Zhang et al., 2011).

Proteomic identification of Kmal peptides

Idenitfying protein substrates is critical to studying the biology of a PTM pathway, as was demonstrated in characterization of the lysine acetylation pathway (Chen et al., 2012; Choudhary et al., 2009; Kim et al., 2006b; Zhao et al., 2010). To identify Kmal substrate proteins and their modification sites, we used a proteomic approach involving affinity enrichment and subsequent HPLC-MS/MS analysis (Fig. 3). Two experimental models were used, namely the SIRT5 KO mice and MCD deficient fibroblasts from malonic aciduria patients. Analysis of Kmal substrates in mouse liver allows us to identify Kmal substrates in this organ important for cellular metabolism (Fig. 3A). The liver also has the highest lysine malonylation levels among the mouse tissues that we screened (Fig. S1). Quantification of Kmal substrates in MCD-deficient cells versus wild-type controls can reveal key Kmal substrates whose modification status is changed in response to malonic aciduria, and whose increased malonylation may play a pathogenic role in this disorder (Fig. 3B).

Protein extracts from liver tissues of SIRT5 KO mice were prepared, tryptically digested, and resolved into 5 fractions by high-pH reversed phase (RP) HPLC. Kmal peptides were enriched using pan α-malonyllysine antibody. The enriched Kmal peptides were analyzed by HPLC-MS/MS (Fig. 3A). The acquired raw MS data were analyzed by MaxQuant software with a false discovery rate (FDR) of 0.01 at protein and peptide level for the identification of Kmal peptides. To ensure high confidence of the identifications, we removed Kmal peptides with Andromeda scores between 40 and 50, and localization probability below 0.75, prior to bioinformatic analysis (Table S1A). The Andromeda score is used for ranking the confidence of peptide identification for the MS/MS spectrum by the Andromeda search engine integrated in Maxquant software. A higher score indicates a more confident peptide identification. This analysis led to identification of 4016 Kmal sites in 1395 proteins in SIRT5 KO mouse liver (Fig. 3C). In a parallel experiment, we identified and quantified Kmal peptides in human dermal fibroblasts isolated from normal individuals ($MCD^{+/+}$, labeled with “Heavy” lysine isotope) and from malonic aciduria patients that are deficient in MCD ($MCD^{-/-}$, labeled with “Light” lysine isotope). Equal amount of protein lysates from both $MCD^{+/+}$ and $MCD^{-/-}$ cells were combined in a 1:1 ratio and processed using the same procedure as described above for analysis of Kmal peptides. The study identified 4943 Kmal sites, with Andromeda scores >50, on 1831 proteins in human fibroblasts ($MCD^{+/+}$ and $MCD^{-/-}$ combined, Fig. 3C).

Among the Kmal substrates, we identified 21 histone marks in mouse liver and 19 histone marks in human fibroblasts. Interestingly, most of them were not located at N-terminal tails of histones (Fig. 3D). Similarly, 35 non-redundant histone lysine succinylation sites have been reported in mouse liver, which mostly localizes to C-terminal globular domains as well (Park et al., 2013). These results suggest that both Kmal and Ksucc histone marks are likely to have differential regulatory function from the widely studied histone acetylation marks.

We previously reported that Ala and Gly were over-represented in the flanking sequences of Ksucc sites, whereas Arg was largely depleted at both -1 and +1

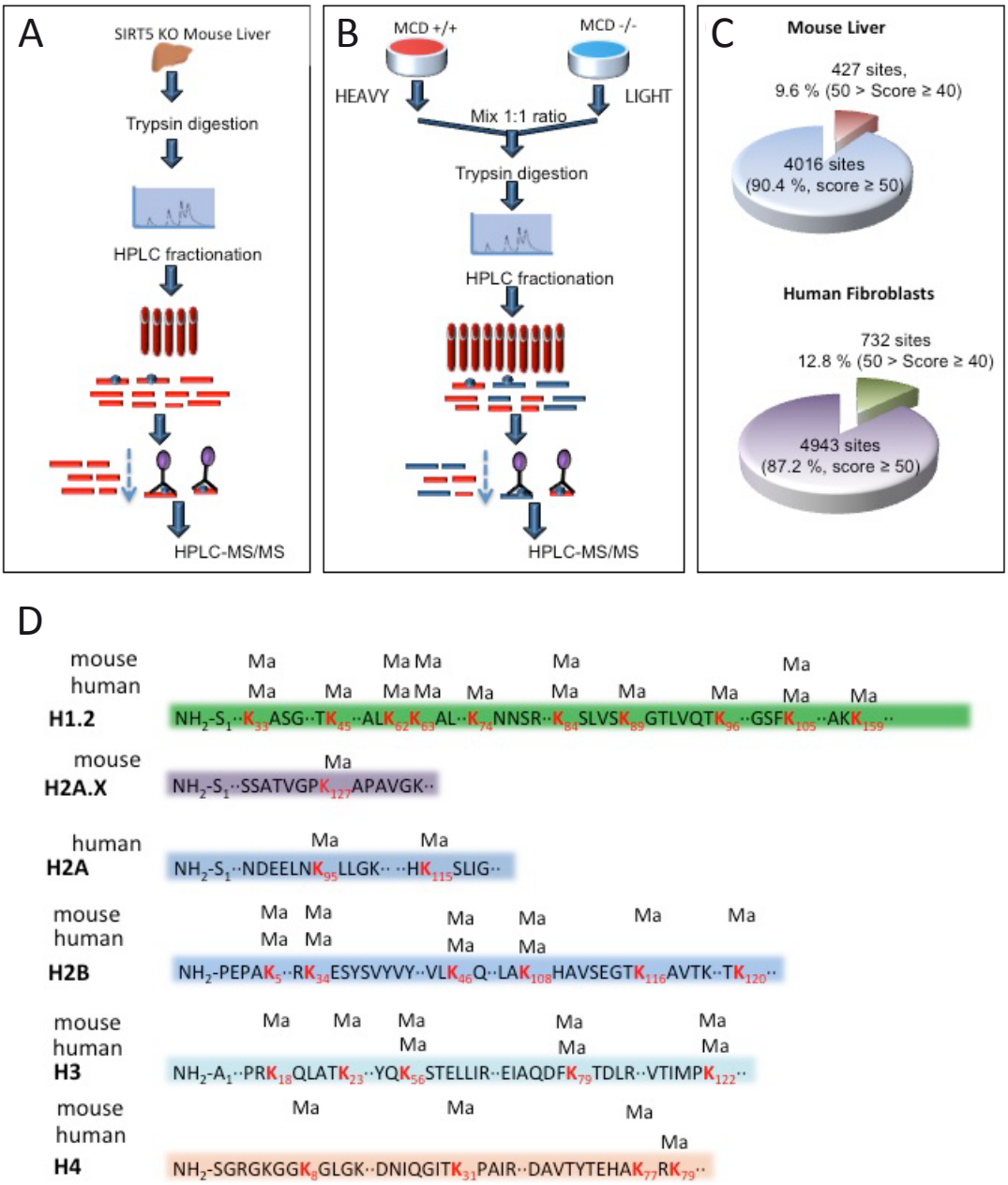

Figure 3. Schematic representation of experimental workflow. (A) Profiling of lysine malonylation substrates in SIRT5 KO mouse liver. (B) Identification and quantification of lysine malonylation substrates, using SILAC and mass spectrometry, in MCD$^{+/+}$ ("Heavy") and MCD$^{-/-}$ ("Light") cell lines. (C) Pie charts showing the total numbers of the identified lysine malonylated sites in mouse liver (top), MCD$^{+/+}$ and MCD$^{-/-}$ human cells (bottom). The number of Kmal sites with their corresponding MaxQuant Andromeda score ranges and percentiles are indicated. (D) Representation of lysine malonylated histone sites in mouse and human histones. A1 and S1 represent the first alanine and serine residues of the protein, respectively.

positions (Park et al., 2013). Similarly, we evaluated the flanking sequences of Kmal sites to identify if there was a structural preference for the location of this modification on the peptides. Motif analyses of Kmal sites in mouse liver (Fig. S2A, left) and human fibroblasts (Fig. S2B, left) showed significant similarity. Aliphatic amino acids, including Ala, Val, Ile and Gly, were over-represented at the flanking sequence of Kmal sites, similar to the situation with Ksucc sites, whereas Ser, Pro and Leu were under-represented. In contrast to the similarity of Kmal and Ksucc flanking sequences, positively charged residues such as Lys and Arg predominate in Kac motifs in mouse liver (Hebert et al., 2013).

Quantification of changes in Kmal modification levels from MCD deficient cell versus its wild type

Using SILAC-based quantitative proteomics approach, we quantified the difference of Kmal substrate levels between $MCD^{+/+}$ and $MCD^{-/-}$ cells, based on the levels of Kmal peptides and those of protein expression. In parallel, we also quantified changes of protein expression using whole cell lysates derived from a mixture of SILAC labeled $MCD^{+/+}$ and $MCD^{-/-}$ cells. The changes of Kmal peptides were then normalized to the change of their corresponding proteins levels in MCD cells. Normalized changes of Kmal peptides were then used for the subsequent analysis.

Among 4943 Kmal sites on 1822 proteins identified in MCD human fibroblasts, 3181 Kmal sites on 1257 proteins could be quantified. Among the 1762 unquantified Kmal sites, 1452 are present only in $MCD^{-/-}$ cells ("Light" only); these are the Kmal peptides that have no detected signal in "Heavy-labeled peptide" (Intensity H) from $MCD^{+/+}$ cells, but significant intensity for the corresponding"Light-labeled peptide (Intensity L)" from $MCD^{-/-}$ cells, by MaxQuant analysis.

The median $MCD^{+/+}$: $MCD^{-/-}$ ratio of the quantifiable Kmal sites was 0.8284 (Fig. 4A). These results clearly suggest that MCD deficiency has a profound impact in elevating Kmal levels in $MCD^{-/-}$ cells. 461 Kmal sites on 339 proteins have increased in abundance by 2 fold or more (normalized log2 ratio ($MCD^{+/+}$: $MCD^{-/-}$) ≤-1), while 1452 Kmal sites on 822 substrate proteins were present in "Light"-only $MCD^{-/-}$ cells (Fig. 4B). 48 Kmal sites on 38 Kmal proteins showed more than a 10-fold increase in $MCD^{-/-}$ cells. We considered these Kmal substrates to represent the core group of Kmal substrates stimulated by MCD deficiency. KEGG pathway analysis indicated that these substrates are associated with the TCA cycle, oxidative phosphorylation, amino acid degradation (valine, leucine, isoleucine, and lysine), fatty acid metabolism and propanoate metabolism pathways.

To calculate the stoichiometry of Kmal in $MCD^{+/+}$ and $MCD^{-/-}$ cells, we modified a reported algorithm (Olsen et al., 2010) as we described previously (Colak et al., 2013; Park et al., 2013). The calculation was based on the successful quantification of a Kmal site, its corresponding protein, and the unmodified peptide form in the SILAC experiment (for details, see (Colak et al., 2013)). To achieve a more accurate calculation, we removed those Kmal sites that were previously reported to be acetylated and succinylated (Weinert et al., 2013b; Wild et al., 2011), to minimize errors caused by the two modifications at the same residues. This analysis enabled

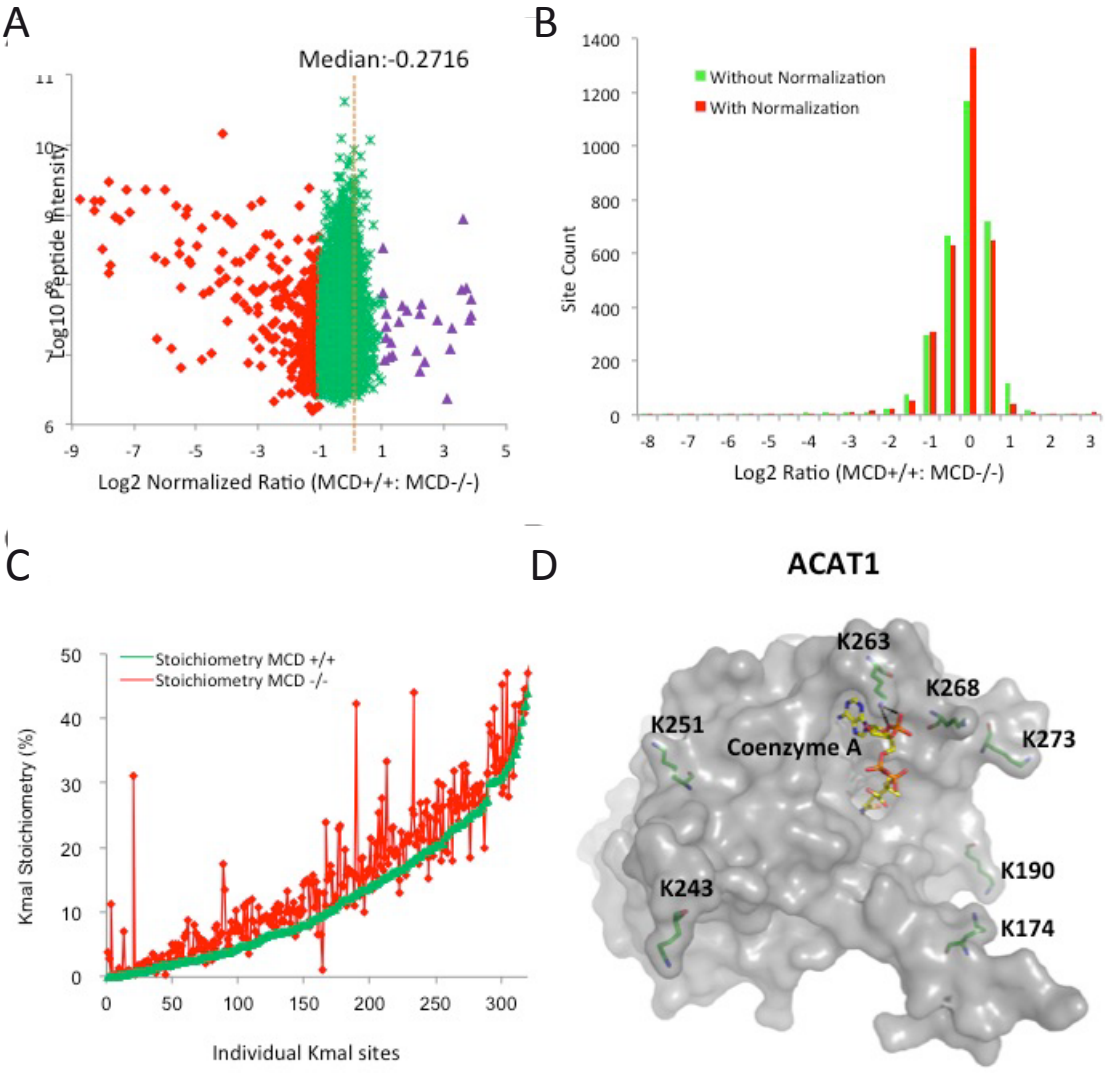

Figure 4. Stoichiometry analysis of lysine malonylome. (A) Scatter plot showing the peptide intensities (i.e., the summed precursor-ion intensities of each peptide, derived from MaxQuant software) of the quantifiable lysine malonylated peptides in relation to their dynamic change in response to MCD knockout. Kmal Ratio ($MCD^{+/+}$: $MCD^{-/-}$): MS signal intensity from $MCD^{+/+}$ divided by that from $MCD^{-/-}$.Red: log2 Ratio ($MCD^{+/+}$:MCD-/-) ≤ -1, Green: -1 ≤ log2 Ratio ($MCD^{+/+}$:$MCD^{-/-}$) ≤ 1; Purple: log2 Ratio ($MCD^{+/+}$:$MCD^{-/-}$) ≥1. (B) Histogram showing the distribution of the log2 ratio ($MCD^{+/+}$:$MCD^{-/-}$) SILAC ratios of Kmal sites in $MCD^{+/+}$ cells over $MCD^{-/-}$ cells. The Y-axis represents the number of Kmal peptides in each category before (green), and after (red) normalization to the protein amount. (C) Stoichiometry analysis of lysine malonylation sites in $MCD^{+/+}$ and $MCD^{-/-}$ human fibroblasts. X-axis represents individual Kmal sites while Y-axis represents the stoichiometry percentage. (D) Three dimensional protein structure of acetyl-CoA acetyltransferase 1 (ACAT1) shown with lysine malonylation sites (K190, K243, K251, K263, K268, K273) and the Co A binding site. Dash black lines represent hydrogen bonds.

us to calculate the stoichiometry of 325 Kmal sites on 222 proteins in $MCD^{-/-}$ cells, with calculated stoichiometries ranging from 0.07% to 50.0% and in $MCD^{+/+}$ cells, with a range from 0.01% to 48.6% (Fig. 4C). The two highest Kmal stoichiometry sites were K376 of adenylyl cyclase-associated protein 1 (50.0% in $MCD^{-/-}$ cells and 48.6% in $MCD^{+/+}$ cells) and K41 of phosphoglycerate kinase (49.4% in $MCD^{-/-}$ cells and 48.2% in $MCD^{+/+}$ cells). Very long chain acyl-CoA dehydrogenase (ACADVL, also known as VLCAD) catalyzes the first step of mitochondrial fatty acid oxidation. Nine Kmal sites were identified in VLCAD, among which five sites were detected in $MCD^{-/-}$ cells only, while the other four were up-regulated in $MCD^{-/-}$ cells, suggesting a dramatic increase of Kmal on this protein. Dynamic increase of two Kmal sites in VLCAD was 390-and 137-fold, respectively, in $MCD^{-/-}$ cells. Among 324 sites whose stoichiometries were determined, 179 sites (55%) have more than a 2-fold increase of Kmal stoichiometry in $MCD^{-/-}$ cells. For example, malonylation at K295 of mitochondrial 10-formyltetrahydrofolate dehydrogenase, responsible for formate oxidation, is increased from 0.7% in $MCD^{+/+}$ cells to 31% in $MCD^{-/-}$ cells. Malonylation at K126 of prohibitin-2, a mediator of transcriptional repression by nuclear hormone receptors, increased from 12.8% to 42.3% in $MCD^{-/-}$ cells.

Overlap among Kmal, Ksucc and Kac sites

To understand the similarities and differences among Kmal, Ksucc, and Kac sites, we compared our lysine malonylome data with previously published data (Chen et al., 2012; Choudhary et al., 2009; Park et al., 2013; Weinert et al., 2013b). We found that of all the identified Kmal sites in mouse liver, 640 (16%) sites (Fig. 5A, right) and 595 (42%) proteins (Fig. 5A, left) overlaped with Kac sites in mouse embryonic fibroblasts (MEF) (Chen et al., 2012), whereas 510 (36.5%) Kmal sites (Fig. 5A, right) and 262 (6.5%) proteins (Fig. 5A, left) overlapped with Ksucc sites in SIRT5 KO mouse liver (Park et al., 2013). When we pooled the Ksucc sites reported in SIRT5 KO mouse liver and MEFs, and carried out the same analysis, 706 (17.6%) sites (Fig. S2C, right) and 406 (29%) proteins (Fig. S2C, left) overlapped with Kmal sites identified in SIRT5 KO mouse liver. Interestingly, we found that a significant portion of the malonylated proteins (46.2%) and sites (71.1%) identified in our mouse liver data do not overlap with the previously reported Ksucc and Kac data.

In a parallel experiment, we carried out a similar analysis for the human malonylome. In this experiment, we obtained the Kac and Ksucc data from previous publications (Choudhary et al., 2009; Weinert et al., 2013b). Among the Kmal sites identified in human fibroblasts (combination of $MCD^{+/+}$ and $MCD^{-/-}$), 776 Kmal sites (Fig. 5B, right) and 827 malonylated proteins (Fig. 5B, left) overlapped with the human Kac proteome (Choudhary et al., 2009), and 671 sites (Fig. 5B, right) and 550 proteins (Fig. 5B, left) overlapped with the human Ksucc proteome (Weinert et al., 2013b). Similar to the mouse malonylome data, a significant portion of the human malonylated proteins (46.7%) and sites (75.7%) did not overlap with previously reported Ksucc and Kac data. Overall, the spectrum of lysine sites and protein targets subject to malonylation shows substantial non-overlap with Kac and Ksucc, suggesting that this modification likely plays roles in modulating biological processes distinct from other lysine PTMs.

Cellular localization of lysine malonylomes

SIRT5, a regulatory enzyme of Ksucc, Kglu, as well as Kmal, localizes predominantly to mitochondria, but is also present in the cytosol and nucleus (Michishita et al., 2005; Park et al., 2013). Previously, we reported that a 17.8% of Ksucc substrates (351) are localized in the mitochondria in mouse liver (Fig. S2F, left) (Park et al., 2013). Among the Ksucc substrates identified in human cervical cancer cells (Hela) (Weinert et al., 2013b), 17% of Ksucc substrates exclusively localizes to mitochondria (Fig. S2F, right).

To understand the cellular localization of Kmal substrates in mouse liver, we performed the same analysis for the Kmal dataset generated from mouse liver. Here, we compared our Kmal dataset with the mitochondria genes annotated in GO database (Pagliarini et al., 2008). Of all the identified Kmal substrates, 316 (58%) of them are present in the mitochondria and 274 (50%) of them are exclusively mitochondrial proteins (Fig. 5C, left). Therefore, a comparable fraction of Kmal and Ksucc proteins from mouse liver localizes to mitochondria.

In parallel, we carried out similar analysis for Kmal proteins derived from human fibroblasts. Our result shows a striking difference of subcellular localization among Kmal substrates. Among the 1024 Kmal substrates identified in human fibroblasts, 338 (33%) of them localize mitochondria, of which 265 (26%) of them are exclusively mitochondrial (Fig. 5C, right). The number of mitochondrial Kmal substrates from either mouse liver or human fibroblasts is comparable. However, in human fibroblasts, we identified a significantly higher number of nuclear and cytosolic substrates, with 262 (30%) and 342 (39%) proteins, respectively (Fig. 5C, right). The cellular enzymes that catalyze lysine malonylation in mammalian cells are still unknown.

Additionally, we compared the Kmal proteins and sites in mitochondria to our previously reported Ksucc data (Park et al., 2013). We found 198 mitochondrial Kmal proteins (13.9% of all Kmal proteins) (Fig. S2D, left) and 432 mitochondrial Kmal sites (10.7% all Kmal sites) (Fig. S2D, right) overlapped with mitochondrial Ksucc in mouse liver, whereas 37% mitochondrial Kmal proteins and 62% Kmal sites did not overlap. In human fibroblasts, 59% mitochondrial Kmal proteins (199) (Fig. S2E, left) and 31% mitochondrial Kmal sites (344) (Fig. S2E, right) overlapped with mitochondrial Ksucc (Weinert et al., 2013b).

We also performed immunostaining of $MCD^{+/+}$ and $MCD^{-/-}$ human fibroblasts with α-malonyllysine, α-acetyllysine and α-succinyllysine antibodies along with Hoechst nuclear stain and MitoTracker Red (Fig. 6A and 6B). Our staining results suggest that the strongest signals for Kac and Ksucc are confined to the nucleus in both $MCD^{+/+}$ and $MCD^{-/-}$ human fibroblasts (Fig. 6A and 6B, 2nd and 3th rows). However, Kmal signals are distributed among the cytosol and nucleus in $MCD^{+/+}$ cells (Fig. 6A, top row). Interestingly, most of the Kmal signal overlaps with MitoTracker Red in $MCD^{-/-}$ cells (Fig. 6B, top row) suggesting that Kmal levels increase specifically in the mitochondria of $MCD^{-/-}$ cells.

Functional annotation of lysine malonylomes

To understand the biological functions of Kmal proteins, we performed

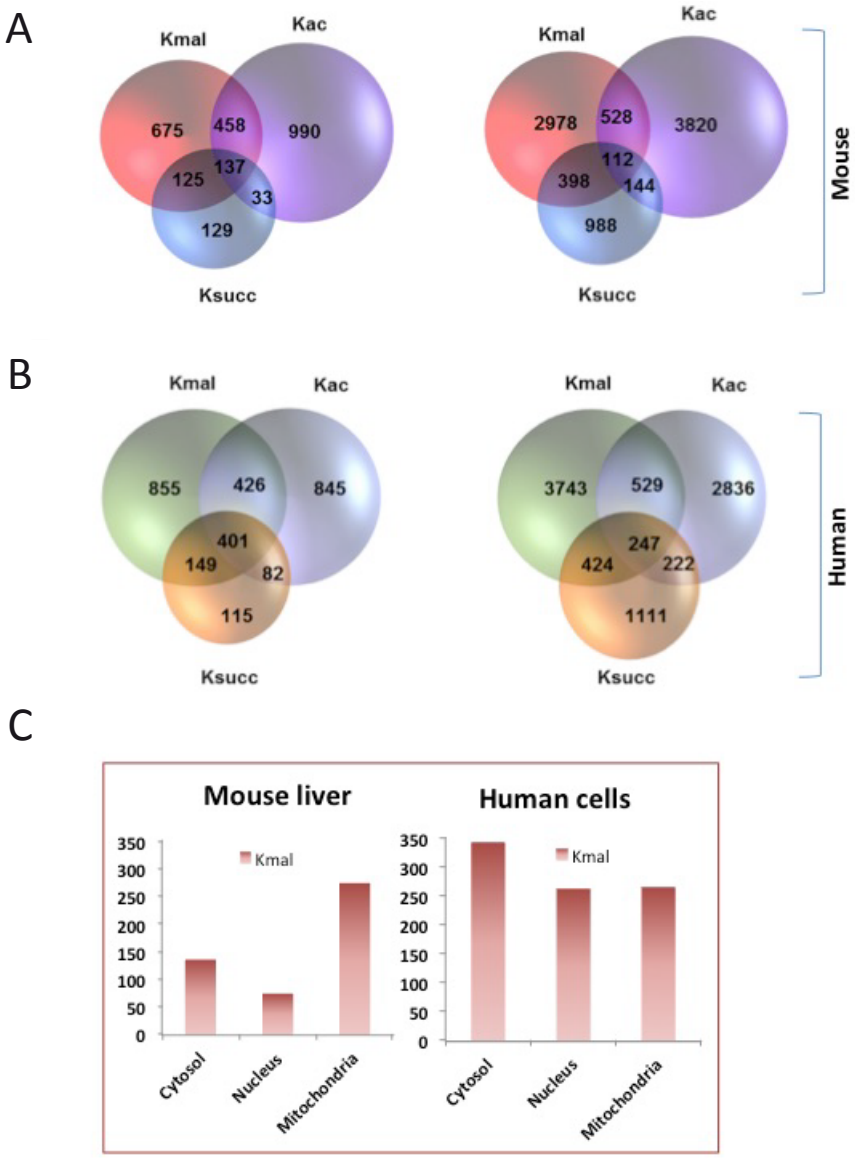

Figure 5. Analysis of Kmal substrates vs Kac and Ksucc substrates. (A) Venn diagrams showing the numbers of overlapping and non-overlapping Kmal, Ksucc and Kac proteins (left) and modification sites (right) in the mouse proteome. The mouse Kac and Ksucc datasets were obtained from two previous publications (Chen et al., 2012; Park et al., 2013). (B) Venn diagrams showing the numbers of overlapping and non-overlapping Kmal, Ksucc and Kac proteins (left) and modification sites (right) in human proteome. All identified Kmal sites in $MCD^{+/+}$ and $MCD^{-/-}$ cells were combined for this comparison. The human Kac and Ksucc datasets were from two previous works (Choudhary et al., 2009; Weinert et al., 2013b). (C) Graphical representation of subcellular localization of lysine malonylated proteins. In each panel, bar diagrams show the numbers of modified proteins that are exclusively located in cytosol, nuclei and mitochondria in mouse liver (left) and human cells (right). See also Fig. S2 and S3.

enrichment analysis by using the Gene Ontology (GO) database (Ashburner et al., 2000), and Kyoto Encyclopedia of Genes and Genomes (KEGG) (Mertins et al., 2013) for Kmal substrates identified in mouse liver and human fibroblasts. The GO biological process analysis of mouse liver Kmal substrates showed enrichment in oxidation/reduction (adj P= 5.45x 10-51), protein translation (adj P = 5.71x 10-49), cofactor metabolism (adj P =4.18x 10-26), and fatty acid metabolism (adj P = 5.09x 10-12) (Fig. S3A, left). The GO analysis of human fibroblast malonylome (Fig. S3B) showed enrichment in protein expression processes such as translation (adj P = 2.22x 10-55), translation elongation (adj P = 7.43x 10-26), tRNA aminoacylation (adj P =1.01x 10-20), and intracellular transport (adj P =5.30x 10-31). Proteins associated with fatty acid β-oxidation were also enriched in the human fibroblast malonylome (adj P =2.34x 10-7).

The molecular function analysis of mouse liver Kmal substrates showed enrichment in nucleotide binding (adj P = 9.35x 10-35), cofactor binding (adj P = 1.04x 10-27), and ATP binding (adj P = 1.86x 10-15) (Fig. S3A, right). Kmal substrates in human fibroblasts were associated with nucleotide binding (adj P = 3.22x 10-45), nucleoside binding (adj P = 2.77x 10-29), ATP binding (adj P = 4.73x 10-26), as well as aminoacyl-tRNA ligase activity (adj P= 2.74x 10-20) (Fig. S3B, right) supporting the idea that Kmal may be involved in regulating protein translation.

There was no significant difference between GO (Fig. S4A) and KEGG pathway enrichments (Fig. S4B) of all the proteins identified in human fibroblasts versus Light-only protein substrates derived from $MCD^{-/-}$ cells. In addition, there was a significant overlap between the KEGG pathway analysis of mouse liver (Fig. S3C) and human fibroblasts (Fig. S3D). The top enriched categories of KEGG pathways for lysine-malonylated substrates were ribosome, valine/leucine/isoleucine degradation, proteasome and fatty acid metabolism (Fig. S3C and S3D). 29 of 45 key enzymes in mouse and 22 of 45 key enzymes in humans involved in regulation of fatty acid metabolism were malonylated, among which five enzymes (FAS, ACC1, ACLY, AMPK and CPT1) are closely associated with malonyl-CoA metabolism.

Of particular note are a few proteins involved in fatty acid metabolism. We found that Acetyl-CoA acetyl transferase 1 (ACAT1), an enzyme participating in multiple metabolic pathways including fatty acid metabolism, was malonylated at seven sites: K174, K190, K243, K251, K263, K268, and K273 (Fig. 4D). The Kmal level of ($MCD^{+/+}$: $MCD^{-/-}$ SILAC ratio of 0.0044) K263 of ACAT1, was increased more than 200-fold in $MCD^{-/-}$ cells. K263 is in close proximity with Coenzyme A binding site and possibly makes two hydrogen bonds with Coenzyme A, suggesting a possibility that this residue is be important in regulating the protein's function. K263 was previously reported to be acetylated and succinylated as well (Choudhary et al., 2009; Weinert et al., 2013b). In addition, among all the Kmal sites of ACAT1, K174 is acetylated, and K251 is succinylated (Choudhary et al., 2009). Therefore, these Kmal sites might also contribute to regulation of protein function, depending on the type of modification. Hydroxymethylglutaryl-CoA lyase (HMGCL) is malonylated at three lysine sites (K48, K93, and K137), of which K48 malonylation is increased roughly 39-fold in $MCD^{-/-}$ cells. HMGCL exclusively localizes to mitochondria and is specifically responsible for leucine degradation, as well as ketone production during fat breakdown. HMGCL

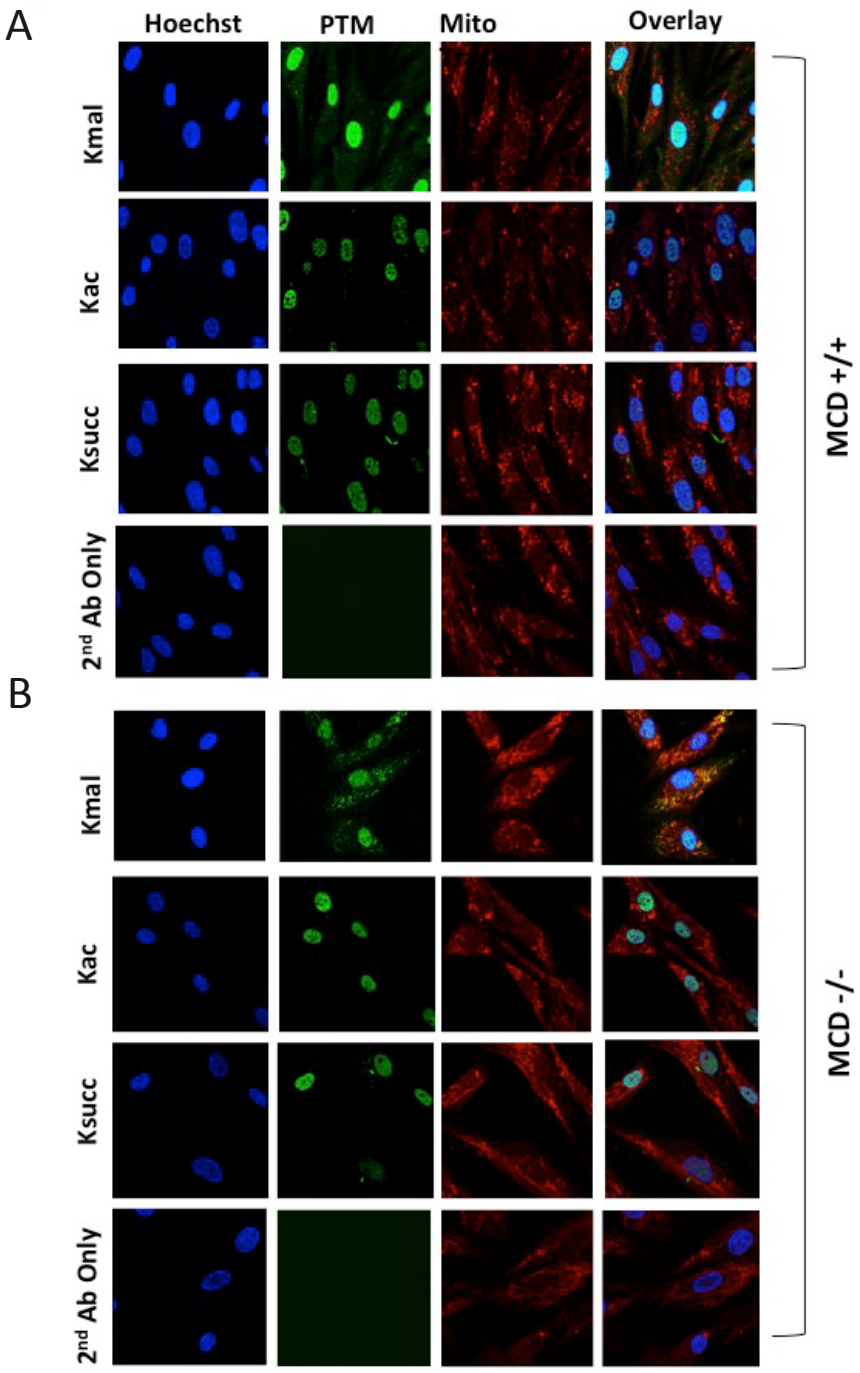

Figure 6. Immunocytochemistry imaging of (A) $MCD^{+/+}$ and (B) $MCD^{-/-}$ cells. Top to bottom: Kmal, Kac and Ksucc staining, and 2nd antibody only (negative) control. Left to right: Hoechst nuclear stain, corresponding PTM, mito-tracker red, and overlapped channels.

deficiency is a rare genetic disease that causes metabolic acidosis and hypoglycemia (Montgomery et al., 2012). A K-to-N mutation at K48 of HMGCL ablates enzymatic activity, which suggests that K48 is a critical position for enzymatic function (Carrasco et al., 2007). Therefore, lysine malonylation of K48 can likely lead to changes in enzymatic activity of this protein. ATP citrate lyase (ACLY) catalyzes conversion of citrate to acetyl-CoA, which can be further converted to malonyl-CoA by ACC1. Among the 14 Kmal sites in ACLY, K68, located next to ATP binding site (K66-K67), is malonylated, and therefore might alter the ATP binding ability of the protein. Enrichment of fatty acid metabolism proteins in the malonylomes in both mouse liver and human fibroblasts suggests a possible feedback regulation of fatty acid biosynthesis by malonyl-CoA-mediated lysine malonylation.

Lysine malonylation impacts mitochondrial function and fatty acid oxidation

Integration of our bioinformatic analyses of lysine malonylated proteins identified in mouse liver and human fibroblast demonstrates that among metabolic pathways, proteins involved in fatty acid metabolism were preferentially heavily malonylated. Fatty acid synthesis, which utilizes malonyl-CoA as substrate for synthesis and chain elongation, primarily occurs in the cytosol, whereas fatty acid oxidation occurs in mitochondria and peroxisomes. Because $MCD^{-/-}$ cells showed greatly increased Kmal immunostaining in mitochondria compared to $MCD^{+/+}$ cells (Fig. 6) and MCD deficient patients have been reported to present with pathologies similar to patients with fatty acid oxidation defects, we wanted to understand whether lysine malonylation in $MCD^{-/-}$ cells would affect mitochondrial function and fatty acid oxidation. Long-chain fatty acids are broken down to medium and short-chain fatty acids in mitochondria by very-long chain acyl-CoA dehydrogenase (VLCAD) and medium-chain acyl-CoA dehydrogenase (MCAD) together with the mitochondrial trifunctional protein (MTP) complex encoded by the HADHA and HADHB genes. MTP complex consists of hydroxyl-acyl-CoA dehydrogenase (LCHAD), long-chain enoyl-CoA hydratase (LCEH), and long-chain keto-acyl-CoA thiolase (LCKAT) enzymatic activities. In $MCD^{-/-}$ cells multiple mitochondrial fatty acid oxidation proteins were heavily malonylated, and both VLCAD and HADHA were substantially more malonylated than in WT cells (Fig. 7A and Fig. S5B). Many of the detectable

Figure 7. Lysine malonylation impacts mitochondrial function and fatty acid oxidation. (A) The SILAC ratios of lysine malonylation sites of VLCAD determined by quantitative proteomics between $MCD^{+/+}$ and $MCD^{-/-}$ fibroblast cells, respectively. A number of malonylated lysines were only detected in $MCD^{-/-}$ cells. (B) VLCAD protein structure with mapped lysine malonylation sites (RCSB protein databank number 2UXW and 3B96). (C) Palmitoyl-CoA dehydrogenase activity of the VLCAD enzyme in cell lysates from $MCD^{+/+}$ and $MCD^{-/-}$ cells. Bars represent means ± standard error of the mean (n=3-6). (D) 3-keto-palmitoyl-CoA dehydrogenase activity of the LCHAD enzyme in cell lysates from $MCD^{+/+}$ and $MCD^{-/-}$ cells. Bars represent means ± standard error of the mean (n=3). (E-G) Respiration analysis of digitonin permeabilized Fao hepatoma cells that were exposed to 50 mM malonate for one day followed by overnight incubation in malonate-free medium (see text for details). Respiration analysis was performed with pyruvate/malate (E), succinate/rotenone (F) or octanoylcarnitine/malate (G). (H-J) Respiration analysis of digitonin permeabilized $MCD^{+/+}$ and $MCD^{-/-}$ fibroblasts similar to F and G. OCR = oxygen consumption rate, OM = oligomycin, AM/rot = antimycin/rotenone. * = p-value <0.05, ** = p-value < 0.01, *** p-value < 0.001. See also Fig. S5.

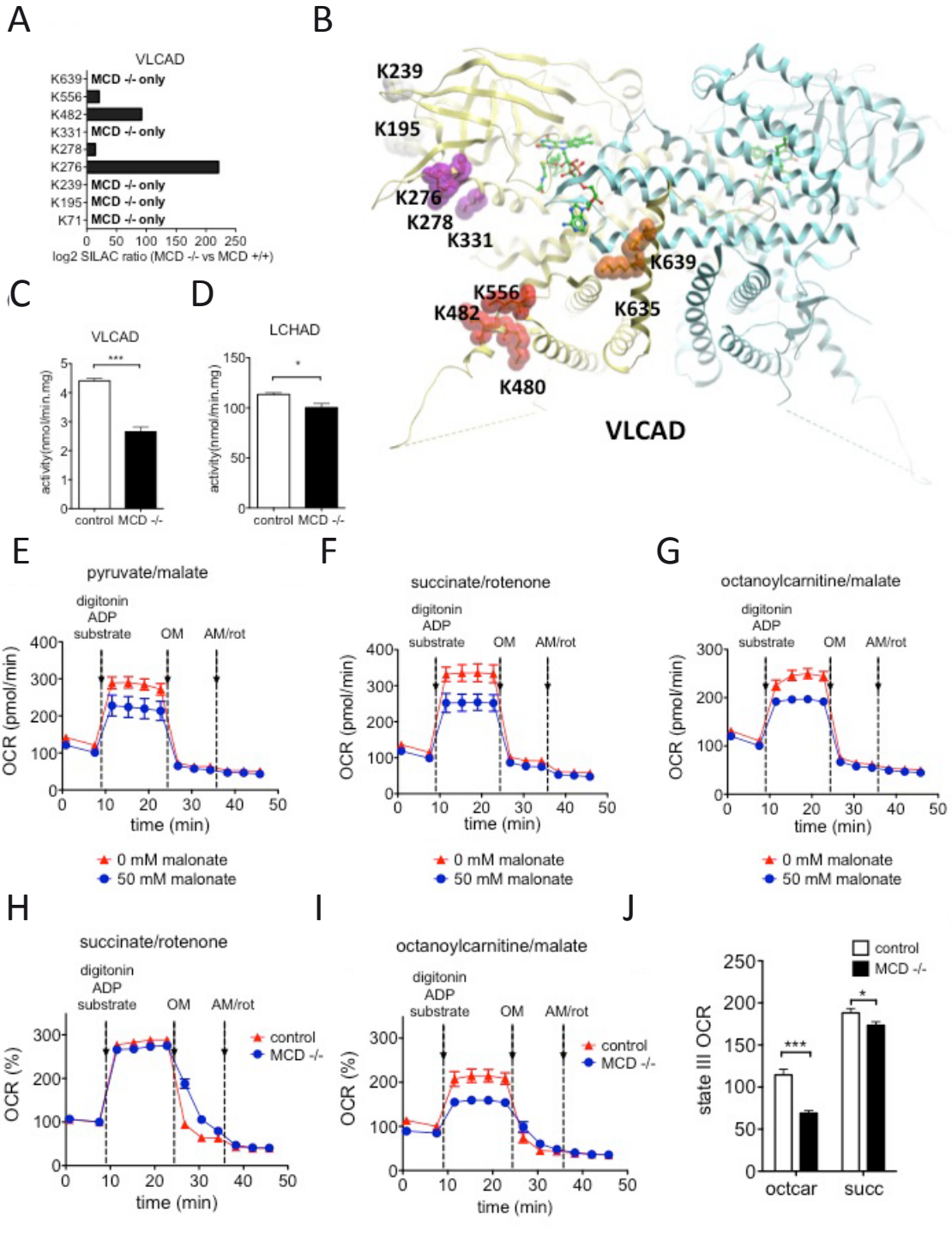
A
VLCAD
K639 MCD -/- only
K556
K482
K331 MCD -/- only
K278
K276
K239 MCD -/- only
K195 MCD -/- only
K71 MCD -/- only
0 50 100 150 200 250
log2 SILAC ratio (MCD -/- vs MCD +/+)
B
K239
K195
K276
K278
K331
K639
K556
K482
K635
K480
VLCAD
C
VLCAD
***
activity(nmol/min.mg)
control MCD -/-
D
LCHAD
*
activity(nmol/min.mg)
control MCD -/-
E
pyruvate/malate
digitonin
ADP
substrate
OM
AM/rot
OCR (pmol/min)
time (min)
0 mM malonate
50 mM malonate
F
succinate/rotenone
digitonin
ADP
substrate
OM
AM/rot
OCR (pmol/min)
time (min)
0 mM malonate
50 mM malonate
G
octanoylcarnitine/malate
digitonin
ADP
substrate
OM
AM/rot
OCR (pmol/min)
time (min)
0 mM malonate
50 mM malonate
H
succinate/rotenone
digitonin
ADP
substrate
OM
AM/rot
OCR (%)
time (min)
control
MCD -/-
I
octanoylcarnitine/malate
digitonin
ADP
substrate
OM
AM/rot
OCR (%)
time (min)
control
MCD -/-
J
control
MCD -/-
state III OCR
***
*
octcar
succ

malonylated lysine sites were only present in $MCD^{-/-}$ cells. Examination of the crystal structure of VLCAD (PDB code 2uxw, 3b96) reveals that sites of lysine malonylation are scattered across the polypeptide (Fig. 7B). Three of the Kmal sites (K278, K331, K480) occupy highly conserved amino acid positions among VLCAD orthologues. A majority of the lysine sites are surface-exposed, and their malonylation may impact different properties of the protein: three (K480, K482, K55) are located at the putative surface of membrane attachment (McAndrew et al., 2008); two (K635, K639) are found in proximity to the dimerization interface, and three (K276, K278, K331) are positioned near the active site where FAD and acyl-CoA molecules bind (Fig. 7B). We next analyzed whether VLCAD enzymatic activity was affected by malonylation in $MCD^{-/-}$ cells. Indeed, VLCAD activity was decreased 45% in $MCD^{-/-}$ cells as compared to $MCD^{+/+}$ cells (Fig. 7C). Basal expression levels of VLCAD protein were similar in $MCD^{+/+}$ and $MCD^{-/-}$ cells (Fig. S5A). Furthermore, the LCHAD activity of MTP was significantly decreased in $MCD^{-/-}$ cells as well (Fig. 7D).

Accumulation of cytosolic malonyl-CoA is known to inhibit CPT1, which is located on the outer membrane of the mitochondria. CPT1, together with CACT and CPT2, imports acyl-CoAs into the mitochondria for beta oxidation. Our data now suggest that accumulation of lysine malonylation on proteins within the mitochondrial matrix can also inhibit fatty acid oxidation. To test if mitochondrial function and fatty acid oxidation are indeed affected by lysine malonylation, we studied impact of malonate on mitochondrial function in Fao liver cells. Previously, we have shown that malonate treatment induces significant lysine malonylation (Peng et al., 2011a). To eliminate any confounding effects from direct interference of malonate itself on mitochondrial function, we treated cells with malonate for one day, followed by a malonate-free overnight incubation, prior to analysis of mitochondrial function. Malonate treatment of cells significantly reduced the oxygen consumption rate (OCR) in the context of pyruvate, succinate and octanoylcarnitine mitochondrial oxidation (Fig. 7E, F and G). CPT1 is not required for oxidation of octanoylcarnitine; hence inhibition of CPT1 by malonyl-CoA cannot explain the observed decrease in OCR in the presence of octanoylcarnitine. Instead, this finding likely indicates that either oxidative phosphorylation or fatty acid oxidation activity is decreased by lysine malonylation.

Finally, we analyzed both succinate and octanoylcarnitine-driven OCR in $MCD^{-/-}$ and $MCD^{+/+}$ cells. Interestingly, succinate-driven OCR was only mildly reduced in $MCD^{-/-}$ cells (Fig. 7H and 7J), whereas octanoylcarnitine-driven OCR was 40% decreased in $MCD^{-/-}$ cells as compared to $MCD^{+/+}$ cells (Fig. 7 I and J). Together, these findings indicate that malonyl-CoA can inhibit mitochondrial fatty acid oxidation in $MCD^{-/-}$ cells, through elevated lysine malonylation, independently of effects on CPT1.

Discussion

In this study, we performed the first global proteomic analysis of the lysine malonylome by using SIRT5 KO mouse liver and human dermal fibroblasts. Overall, we identified 4042 lysine malonylated peptides in 1426 proteins in SIRT5 KO mouse liver, and 4943 malonylated peptides in 1822 proteins in human fibroblasts. Four

hundred sixty-one Kmal sites on 339 proteins showed a 2-fold increase or more in $MCD^{-/-}$ cells relative to $MCD^{+/+}$ cells, and 1452 Kmal sites on 822 proteins were only detected in $MCD^{-/-}$ cells, suggests that MCD activity has a profound impact on Kmal levels.

Our analysis revealed intriguing differences between Kmal substrates versus other lysine PTMs (Choudhary et al., 2009; Park et al., 2013). First, Kmal substrates show divergent cellular localization patterns between liver and fibroblast cells (Fig. 5C). In mouse liver, Kmal and Ksucc predominantly localized to mitochondria, with a small number of substrate proteins in the cytosol and nucleus. In contrast, in the case of $MCD^{+/+}$ human fibroblasts, Kmal proteins were distributed among cytosol and nucleus (Fig. 5C, right), whereas in $MCD^{-/-}$ cells, increased localization of Kmal substrates in the mitochondria was observed. Malonyl-CoA is reported to localize to extracellular, membrane, mitochondrial and peroxisomal spaces of the cell according to the Human Metabolome Database (http://www.hmdb.ca/metabolites/hmdb01175). The concentration of malonyl-CoA in mitochondria is not known. It is likely that mitochondrial malonyl-CoA is the cofactor for lysine malonylation reaction.

Second, the identification of a large number of Kmal substrates in the cytosol and nucleus of human fibroblasts suggests the potential existence of enzyme(s) catalyzing the transfer of malonyl groups from malonyl-CoA to lysine residues. It has been proposed that this process occurs non-enzymatically in the high-pH chemical environment of mitochondria (Wagner and Hirschey, 2014; Wagner and Payne, 2013; Weinert et al., 2013b). However, this *in vitro* spontaneous protein acylation cannot exclude the possibility of an enzyme-catalyzed PTM reaction, as in the case of lysine acetylation, which can occur via both non-enzymatic and enzyme-catalyzed reactions. Given the fact that the pH is lower in the cytosol and nucleus than in mitochondria, and that the subcellular localization of Kmal substrates is very different in liver versus fibroblasts, it is possible that there is significant enzyme-catalyzed lysine malonylation outside of mitochondria in human fibroblasts.

Third, 2693 Kmal sites remain at similar levels (with less than a 2-fold change) in human fibroblasts, unaffected by the expression of MCD enzyme. Cellular localization analysis showed that these Kmal substrates were not enriched in mitochondria. In stark contrast, the proteins showing increased Kmal in MCD deficiency (more than 2 fold change) were enriched in the mitochondria. This suggests that the increased Kmal occurring in the context of MCD deficiency primarily impacts mitochondrial functions, including mitochondrial respiration. Indeed, we showed that lysine malonylation inhibited mitochondrial function and impaired octanoylcarnitine oxidation in $MCD^{-/-}$ cells. Because mitochondrial octanoylcarnitine oxidation does not require CPT1, our studies demonstrate that malonyl-CoA can also impact fatty acid oxidation and mitochondrial function via malonylation of proteins located in the mitochondrial matrix, independently of CPT1. This implies that malonyl-CoA can play a major role in controlling mitochondrial function by lysine malonylation of mitochondrial matrix proteins.

Diverse pathological symptoms have been observed in patients with inborn MCD deficiency, several of which are also common in fatty acid oxidation disorders, such

as cardiomyopathy, muscle weakness and hypoglycemia (Houten and Wanders, 2010; Salomons et al., 2007). This observation has led to the hypothesis that CPT1 inhibition by elevated malonyl-CoA levels could play a role in the pathophysiology of MCD deficiency. Indeed, palmitate and myristate oxidation was severely reduced in MCD deficient patient fibroblasts, implying a likely role of malonyl-CoA in inhibition of fatty acid oxidation in pathogenesis of this disorder (Bennett et al., 2001). In light of our result that malonyl-CoA accumulation can impact metabolic pathways via CPT1-independent lysine malonylation, it seems likely that accumulation of mitochondrial lysine malonylation also plays a pathogenic role in MCD deficiency. Moreover, KEGG pathway analysis of Kmal substrates showed enrichment of the modification in pathways besides those associated with fatty acid metabolism. MCD deficient patients can suffer from delayed neurological development (de Wit et al., 2006). Although the pathogenic mechanism of this effect is still not well understood, it has been suggested that disruption of the interaction between malonyl-CoA and CPT1 might be a cause (Malvagia et al., 2007). Our data suggest that elevated Kmal on many mitochondrial proteins may represent another mechanism of the neuropathology associated with malonic aciduria. Since Kmal levels are regulated by SIRT5, this raises the possibility that pharmacologic strategies to increase SIRT5 activity may represent a rational treatment strategy in MCD deficiency.

Identification, characterization and proteomic screening of three acidic lysine acylation pathways suggest association of these pathways with multiple inborn metabolic diseases. In this study, our results suggest that elevated malonic acid in MCD deficient cells might induce Kmal levels in substrate proteins that in turn impair the activities of key cellular metabolic enzymes, such as VLCAD and LCHAD. Glutaric Acidemia I (GA, OMIM: 231670) is caused by homozygous or compound heterozygous mutations in the gene encoding glutaryl-CoA dehydrogenase (GCDH). A previous study demonstrated that GA patients as well as GCDH KO mice display increased levels of glutaryl-CoA (Koeller et al., 2002). We showed that glutarylation suppresses CPS1 enzymatic activity in cell lines, mice, and a model of glutaric academia type I disease. This result suggests that up-regulation of glutaric acid and glutaryl-CoA leads to elevated levels of Kglu that in turn modulate activities of substrate proteins (Tan et al., 2014). Furthermore, we previously demonstrated that lysine propionylation and lysine butyrylation also accumulate in propionyl-CoA carboxylase (PCC) deficiency and short-chain acyl-CoA dehydrogenase (SCAD) deficiency, respectively (Pougovkina et al., 2014). Additionally, mutations in the genes that are involved in succinyl-CoA metabolism, such as ketoglutarate dehydrogenase, succinyl-CoA–3-ketoacid-Co-A transferase and succinyl-CoA ligase, lead to metabolic diseases (Ostergaard, 2008). Weinert et al. demonstrated that loss of succinyl-CoA ligase in yeast results in increased lysine succinylation, suggesting that accumulation of mitochondrial succinyl-CoA also increases mitochondrial succinylation (Weinert et al., 2013b). Taken together, a new concept has emerged from studies of these acidic lysine acylations: genetic defects in enzymes involved in the metabolism of acyl-CoA species and/or their corresponding acylic acids can lead to elevated cellular acyl-CoA concentrations. Elevated levels of acyl-CoA in turn induce lysine acylation in substrate proteins that can modulate their functions and

even contribute to disease.

Mechanistic understanding of Kmal, Ksucc, and Kglu pathway dysregulation in inborn metabolic diseases may be relevant for developing novel therapeutic strategies for these diseases. For example, it may be possible to activate SIRT5 and alleviate the symptomatology in these conditions. Moreover, this mechanistic understanding can be instrumental for the analysis of the role of lysine acylation in other diseases, like diabetes and cancer, where disturbance of metabolic homeostasis plays a critical role.

References

Abu-Elheiga, L., Oh, W., Kordari, P., and Wakil, S.J. (2003). Acetyl-CoA carboxylase 2 mutant mice are protected against obesity and diabetes induced by high-fat/high-carbohydrate diets. Proceedings of the National Academy of Sciences of the United States of America 100, 10207-10212.

Ashburner, M., Ball, C.A., Blake, J.A., Botstein, D., Butler, H., Cherry, J.M., Davis, A.P., Dolinski, K., Dwight, S.S., Eppig, J.T., et al. (2000). Gene ontology: tool for the unification of biology. The Gene Ontology Consortium. Nature genetics 25, 25-29.

Bandyopadhyay, G.K., Yu, J.G., Ofrecio, J., and Olefsky, J.M. (2006). Increased malonyl-CoA levels in muscle from obese and type 2 diabetic subjects lead to decreased fatty acid oxidation and increased lipogenesis; thiazolidinedione treatment reverses these defects. Diabetes 55, 2277-2285.

Bennett, M.J., Harthcock, P.A., Boriack, R.L., and Cohen, J.C. (2001). Impaired mitochondrial fatty acid oxidative flux in fibroblasts from a patient with malonyl-CoA decarboxylase deficiency. Molecular genetics and metabolism 73, 276-279.

Carrasco, P., Menao, S., Lopez-Vinas, E., Santpere, G., Clotet, J., Sierra, A.Y., Gratacos, E., Puisac, B., Gomez-Puertas, P., Hegardt, F.G., et al. (2007). C-terminal end and aminoacid Lys48 in HMG-CoA lyase are involved in substrate binding and enzyme activity. Molecular genetics and metabolism 91, 120-127.

Chang, H.C., and Guarente, L. (2014). SIRT1 and other sirtuins in metabolism. Trends in endocrinology and metabolism: TEM 25, 138-145.

Chen, Y., Zhao, W., Yang, J.S., Cheng, Z., Luo, H., Lu, Z., Tan, M., Gu, W., and Zhao, Y. (2012). Quantitative acetylome analysis reveals the roles of SIRT1 in regulating diverse substrates and cellular pathways. Molecular & cellular proteomics : MCP 11, 1048-1062.

Choudhary, C., Kumar, C., Gnad, F., Nielsen, M.L., Rehman, M., Walther, T.C., Olsen, J.V., and Mann, M. (2009). Lysine acetylation targets protein complexes and co-regulates major cellular functions. Science 325, 834-840.

Colaert, N., Helsens, K., Martens, L., Vandekerckhove, J., and Gevaert, K. (2009). Improved visualization of protein consensus sequences by iceLogo. Nature methods 6, 786-787.

Colak, G., Xie, Z., Zhu, A.Y., Dai, L., Lu, Z., Zhang, Y., Wan, X., Chen, Y., Cha, Y.H., Lin, H., et al. (2013). Identification of lysine succinylation substrates and the succinylation regulatory enzyme CobB in Escherichia coli. Molecular & cellular proteomics : MCP 12, 3509-3520.

Dai, L., Peng, C., Montellier, E., Lu, Z., Chen, Y., Ishii, H., Debernardi, A., Buchou, T., Rousseaux, S., Jin, F., et al. (2014). Lysine 2-hydroxyisobutyrylation is a widely distributed active histone mark. Nature chemical biology 10, 365-370.

de Wit, M.C., de Coo, I.F., Verbeek, E., Schot, R., Schoonderwoerd, G.C., Duran, M., de Klerk, J.B., Huijmans, J.G., Lequin, M.H., Verheijen, F.W., et al. (2006). Brain abnormalities in a case of malonyl-CoA decarboxylase deficiency. Molecular genetics and metabolism 87, 102-106.

Du, J., Zhou, Y., Su, X., Yu, J.J., Khan, S., Jiang, H., Kim, J., Woo, J., Kim, J.H., Choi, B.H., et al. (2011). Sirt5 is a NAD-dependent protein lysine demalonylase and desuccinylase. Science 334, 806-809.

Fillmore, N., and Lopaschuk, G.D. (2014). Malonyl CoA: A promising target for the treatment of cardiac disease. IUBMB life.

FitzPatrick, D.R., Hill, A., Tolmie, J.L., Thorburn, D.R., and Christodoulou, J. (1999). The molecular basis of malonyl-CoA decarboxylase deficiency. American journal of human genetics 65, 318-326.

Giblin, W., Skinner, M.E., and Lombard, D.B. (2014). Sirtuins: guardians of mammalian healthspan. Trends in genetics : TIG 30, 271-286.

Haberland, M., Montgomery, R.L., and Olson, E.N. (2009). The many roles of histone deacetylases in development and physiology: implications for disease and therapy. Nature reviews Genetics 10, 32-42.

Hebert, A.S., Dittenhafer-Reed, K.E., Yu, W., Bailey, D.J., Selen, E.S., Boersma, M.D., Carson, J.J., Tonelli, M., Balloon, A.J., Higbee, A.J., et al. (2013). Calorie restriction and SIRT3 trigger global reprogramming of the mitochondrial protein acetylome. Molecular cell 49, 186-199.

Houten, S.M., and Wanders, R.J. (2010). A general introduction to the biochemistry of mitochondrial

fatty acid beta-oxidation. Journal of inherited metabolic disease 33, 469-477.

Huang da, W., Sherman, B.T., and Lempicki, R.A. (2009). Bioinformatics enrichment tools: paths toward the comprehensive functional analysis of large gene lists. Nucleic acids research 37, 1-13.

Jensen, L.J., Kuhn, M., Stark, M., Chaffron, S., Creevey, C., Muller, J., Doerks, T., Julien, P., Roth, A., Simonovic, M., et al. (2009). STRING 8--a global view on proteins and their functional interactions in 630 organisms. Nucleic acids research 37, D412-416.

Kanehisa, M., and Goto, S. (2000). KEGG: kyoto encyclopedia of genes and genomes. Nucleic acids research 28, 27-30.

Kim, S.C., Chen, Y., Mirza, S., Xu, Y., Lee, J., Liu, P., and Zhao, Y. (2006a). A clean, more efficient method for in-solution digestion of protein mixtures without detergent or urea. Journal of proteome research 5, 3446-3452.

Kim, S.C., Sprung, R., Chen, Y., Xu, Y., Ball, H., Pei, J., Cheng, T., Kho, Y., Xiao, H., Xiao, L., et al. (2006b). Substrate and functional diversity of lysine acetylation revealed by a proteomics survey. Molecular cell 23, 607-618.

Koeller, D.M., Woontner, M., Crnic, L.S., Kleinschmidt-DeMasters, B., Stephens, J., Hunt, E.L., and Goodman, S.I. (2002). Biochemical, pathologic and behavioral analysis of a mouse model of glutaric acidemia type I. Human molecular genetics 11, 347-357.

Kridel, S.J., Axelrod, F., Rozenkrantz, N., and Smith, J.W. (2004). Orlistat is a novel inhibitor of fatty acid synthase with antitumor activity. Cancer research 64, 2070-2075.

Lee, J.H., Choy, M.L., and Marks, P.A. (2012). Mechanisms of resistance to histone deacetylase inhibitors. Advances in cancer research 116, 39-86.

Lombard, D.B., Alt, F.W., Cheng, H.L., Bunkenborg, J., Streeper, R.S., Mostoslavsky, R., Kim, J., Yancopoulos, G., Valenzuela, D., Murphy, A., et al. (2007). Mammalian Sir2 homolog SIRT3 regulates global mitochondrial lysine acetylation. Molecular and cellular biology 27, 8807-8814.

Malvagia, S., Papi, L., Morrone, A., Donati, M.A., Ciani, F., Pasquini, E., la Marca, G., Scholte, H.R., Genuardi, M., and Zammarchi, E. (2007). Fatal malonyl CoA decarboxylase deficiency due to maternal uniparental isodisomy of the telomeric end of chromosome 16. Annals of human genetics 71, 705-712.

McAndrew, R.P., Wang, Y., Mohsen, A.W., He, M., Vockley, J., and Kim, J.J. (2008). Structural basis for substrate fatty acyl chain specificity: crystal structure of human very-long-chain acyl-CoA dehydrogenase. The Journal of biological chemistry 283, 9435-9443.

Mertins, P., Qiao, J.W., Patel, J., Udeshi, N.D., Clauser, K.R., Mani, D.R., Burgess, M.W., Gillette, M.A., Jaffe, J.D., and Carr, S.A. (2013). Integrated proteomic analysis of post-translational modifications by serial enrichment. Nature methods 10, 634-637.

Michishita, E., Park, J.Y., Burneskis, J.M., Barrett, J.C., and Horikawa, I. (2005). Evolutionarily conserved and nonconserved cellular localizations and functions of human SIRT proteins. Molecular biology of the cell 16, 4623-4635.

Montgomery, C., Pei, Z., Watkins, P.A., and Miziorko, H.M. (2012). Identification and characterization of an extramitochondrial human 3-hydroxy-3-methylglutaryl-CoA lyase. The Journal of biological chemistry 287, 33227-33236.

Nakagawa, T., Lomb, D.J., Haigis, M.C., and Guarente, L. (2009). SIRT5 Deacetylates carbamoyl phosphate synthetase 1 and regulates the urea cycle. Cell 137, 560-570.

Nouws, J., Nijtmans, L., Houten, S.M., van den Brand, M., Huynen, M., Venselaar, H., Hoefs, S., Gloerich, J., Kronick, J., Hutchin, T., et al. (2010). Acyl-CoA dehydrogenase 9 is required for the biogenesis of oxidative phosphorylation complex I. Cell metabolism 12, 283-294.

Olsen, J.V., Vermeulen, M., Santamaria, A., Kumar, C., Miller, M.L., Jensen, L.J., Gnad, F., Cox, J., Jensen, T.S., Nigg, E.A., et al. (2010). Quantitative phosphoproteomics reveals widespread full phosphorylation site occupancy during mitosis. Science signaling 3, ra3.

Ostergaard, E. (2008). Disorders caused by deficiency of succinate-CoA ligase. Journal of inherited metabolic disease 31, 226-229.

Pagliarini, D.J., Calvo, S.E., Chang, B., Sheth, S.A., Vafai, S.B., Ong, S.E., Walford, G.A., Sugiana, C., Boneh, A., Chen, W.K., et al. (2008). A mitochondrial protein compendium elucidates complex I disease biology. Cell 134, 112-123.

Park, J., Chen, Y., Tishkoff, D.X., Peng, C., Tan, M., Dai, L., Xie, Z., Zhang, Y., Zwaans, B.M., Skinner, M.E., et al. (2013). SIRT5-mediated lysine desuccinylation impacts diverse metabolic pathways. Molecular cell 50, 919-930.

Peng, C., Lu, Z., Xie, Z., Cheng, Z., Chen, Y., Tan, M., Luo, H., Zhang, Y., He, W., Yang, K., et al. (2011). The first identification of lysine malonylation substrates and its regulatory enzyme. Molecular & cellular proteomics : MCP, M111 012658.

Pougovkina, O., Te Brinke, H., Wanders, R.J., Houten, S.M., and de Boer, V.C. (2014). Aberrant protein acylation is a common observation in inborn errors of acyl-CoA metabolism. Journal of inherited metabolic disease 37, 3513-3522.

Roth, S.Y., Denu, J.M., and Allis, C.D. (2001). Histone acetyltransferases. Annual review of biochemistry 70, 81-120.

Saggerson, D. (2008). Malonyl-CoA, a key signaling molecule in mammalian cells. Annual review of nutrition 28, 253-272.

Salabei, J.K., Gibb, A.A., and Hill, B.G. (2014). Comprehensive measurement of respiratory activity in permeabilized cells using extracellular flux analysis. Nature protocols 9, 421-438.

Salomons, G.S., Jakobs, C., Pope, L.L., Errami, A., Potter, M., Nowaczyk, M., Olpin, S., Manning, N., Raiman, J.A., Slade, T., et al. (2007). Clinical, enzymatic and molecular characterization of nine new patients with malonyl-coenzyme A decarboxylase deficiency. Journal of inherited metabolic disease 30, 23-28.

Santer, R., Fingerhut, R., Lassker, U., Wightman, P.J., Fitzpatrick, D.R., Olgemoller, B., and Roscher, A.A. (2003). Tandem mass spectrometric determination of malonylcarnitine: diagnosis and neonatal screening of malonyl-CoA decarboxylase deficiency. Clinical chemistry 49, 660-662.

Tan, M., Luo, H., Lee, S., Jin, F., Yang, J.S., Montellier, E., Buchou, T., Cheng, Z., Rousseaux, S., Rajagopal, N., et al. (2011). Identification of 67 histone marks and histone lysine crotonylation as a new type of histone modification. Cell 146, 1016-1028.

Tan, M., Peng, C., Anderson, K.A., Chhoy, P., Xie, Z., Dai, L., Park, J., Chen, Y., Huang, H., Zhang, Y., et al. (2014). Lysine glutarylation is a protein posttranslational modification regulated by SIRT5. Cell metabolism 19, 605-617.

Tong, L., and Harwood, H.J., Jr. (2006). Acetyl-coenzyme A carboxylases: versatile targets for drug discovery. Journal of cellular biochemistry 99, 1476-1488.

Wagner, G.R., and Hirschey, M.D. (2014). Nonenzymatic protein acylation as a carbon stress regulated by sirtuin deacylases. Molecular cell 54, 5-16.

Wagner, G.R., and Payne, R.M. (2013). Widespread and enzyme-independent Nepsilon-acetylation and Nepsilon-succinylation of proteins in the chemical conditions of the mitochondrial matrix. The Journal of biological chemistry 288, 29036-29045.

Wanders, R.J., L, I.J., van Gennip, A.H., Jakobs, C., de Jager, J.P., Dorland, L., van Sprang, F.J., and Duran, M. (1990). Long-chain 3-hydroxyacyl-CoA dehydrogenase deficiency: identification of a new inborn error of mitochondrial fatty acid beta-oxidation. Journal of inherited metabolic disease 13, 311-314.

Weinert, B.T., Scholz, C., Wagner, S.A., Iesmantavicius, V., Su, D., Daniel, J.A., and Choudhary, C. (2013). Lysine succinylation is a frequently occurring modification in prokaryotes and eukaryotes and extensively overlaps with acetylation. Cell reports 4, 842-851.

Wild, P., Farhan, H., McEwan, D.G., Wagner, S., Rogov, V.V., Brady, N.R., Richter, B., Korac, J., Waidmann, O., Choudhary, C., et al. (2011). Phosphorylation of the autophagy receptor optineurin restricts Salmonella growth. Science 333, 228-233.

Wolfgang, M.J., and Lane, M.D. (2008). Hypothalamic malonyl-coenzyme A and the control of energy balance. Molecular endocrinology 22, 2012-2020.

Xie, Z., Dai, J., Dai, L., Tan, M., Cheng, Z., Wu, Y., Boeke, J.D., and Zhao, Y. (2012). Lysine succinylation and lysine malonylation in histones. Molecular & cellular proteomics : MCP 11, 100-107.

Yang, X.J., and Seto, E. (2007). HATs and HDACs: from structure, function and regulation to novel strategies for therapy and prevention. Oncogene 26, 5310-5318.

Zhang, Z., Tan, M., Xie, Z., Dai, L., Chen, Y., and Zhao, Y. (2011). Identification of lysine succinylation as a new post-translational modification. Nature chemical biology 7, 58-63.

Zhao, S., Xu, W., Jiang, W., Yu, W., Lin, Y., Zhang, T., Yao, J., Zhou, L., Zeng, Y., Li, H., et al. (2010). Regulation of cellular metabolism by protein lysine acetylation. Science 327, 1000-1004.

Supplementary Figures

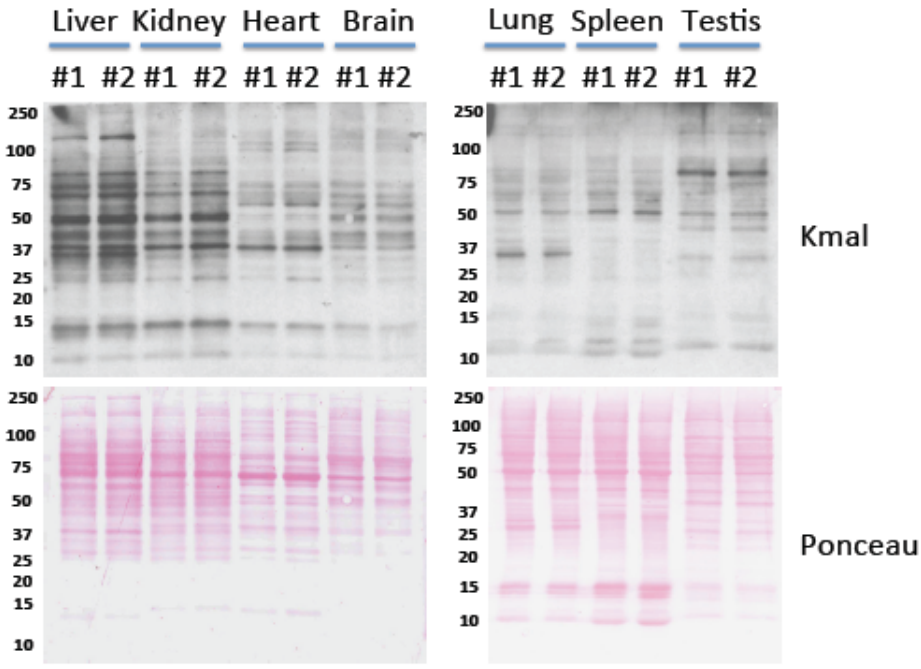

Figure S1 (Related to Figure 2). Western blot analysis of Kmal levels in mouse liver, kidney, heart, brain, lung, spleen and testis tissues obtained from two C57BL6 male mice (#1-2). Top, α-malonyllysine blot; bottom, Ponseau staining for loading control.

Figure S2 (Related to Figure 5). (A) Left: Schematic representation for the motif analysis of lysine malonylated sites from mouse liver by iceLogo. Right: Pie chart showing the percentage of total lysine malonylation sites per protein in mouse liver. (B) Left: Schematic representation for the motif analysis of lysine malonylated sites in human fibroblasts ($MCD^{+/+}$ and $MCD^{-/-}$ data combined). Right: Pie chart showing the percentage of total lysine malonylation sites per protein in human fibroblasts ($MCD^{+/+}$ and $MCD^{-/-}$ data combined). (C) Venn diagrams showing the numbers of overlapping and non-overlapping Kmal, Ksucc and Kac proteins (left) and modification sites (right) in mouse proteome. For this analysis, we combined all the identified Ksucc sites in mouse liver and MEF cells. The Ksucc dataset used is from Park et al. (Park et al., 2013) while the Kac dataset used is from Chen et al. (Chen et al., 2012). (D) and (E). Schematic representation of the overlapping mitochondrial Kmal proteins (left) and modification sites (right) with mitochondrial Ksucc proteins (left) and modification sites (right), in mouse liver (D) and human fibroblasts (E). (F) Graphical representation of subcellular localization of lysine succinylated proteins. In each panel, bar diagrams show the numbers of modified proteins that are exclusively located in cytosol, nuclei and mitochondria in mouse liver (left) and human cells (right).

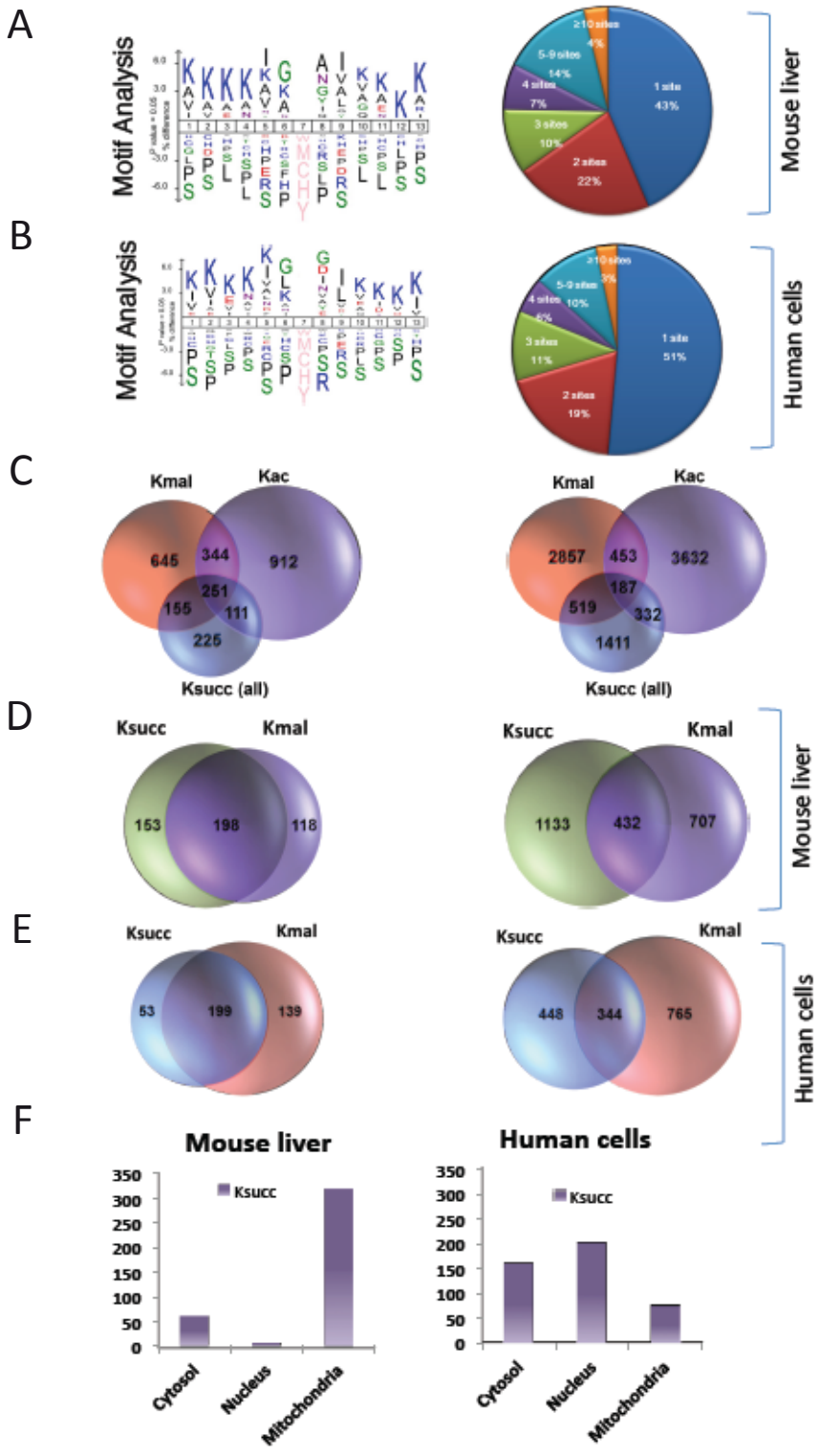
A
Motif Analysis
≥10 sites
4%
5-9 sites
14%
4 sites
7%
3 sites
10%
2 sites
22%
1 site
43%
Mouse liver
B
Motif Analysis
≥10 sites
5%
5-9 sites
10%
4 sites
6%
3 sites
11%
2 sites
19%
1 site
51%
Human cells
C
Kmal
Kac
645
344
912
251
155
111
225
Ksucc (all)
Kmal
Kac
2857
453
3632
187
519
332
1411
Ksucc (all)
D
Ksucc
Kmal
153
198
118
Ksucc
Kmal
1133
432
707
Mouse liver
E
Ksucc
Kmal
53
199
139
Ksucc
Kmal
448
344
765
Human cells
F
Mouse liver
Ksucc
350
300
250
200
150
100
50
0
Cytosol
Nucleus
Mitochondria
Human cells
Ksucc
350
300
250
200
150
100
50
0
Cytosol
Nucleus
Mitochondria

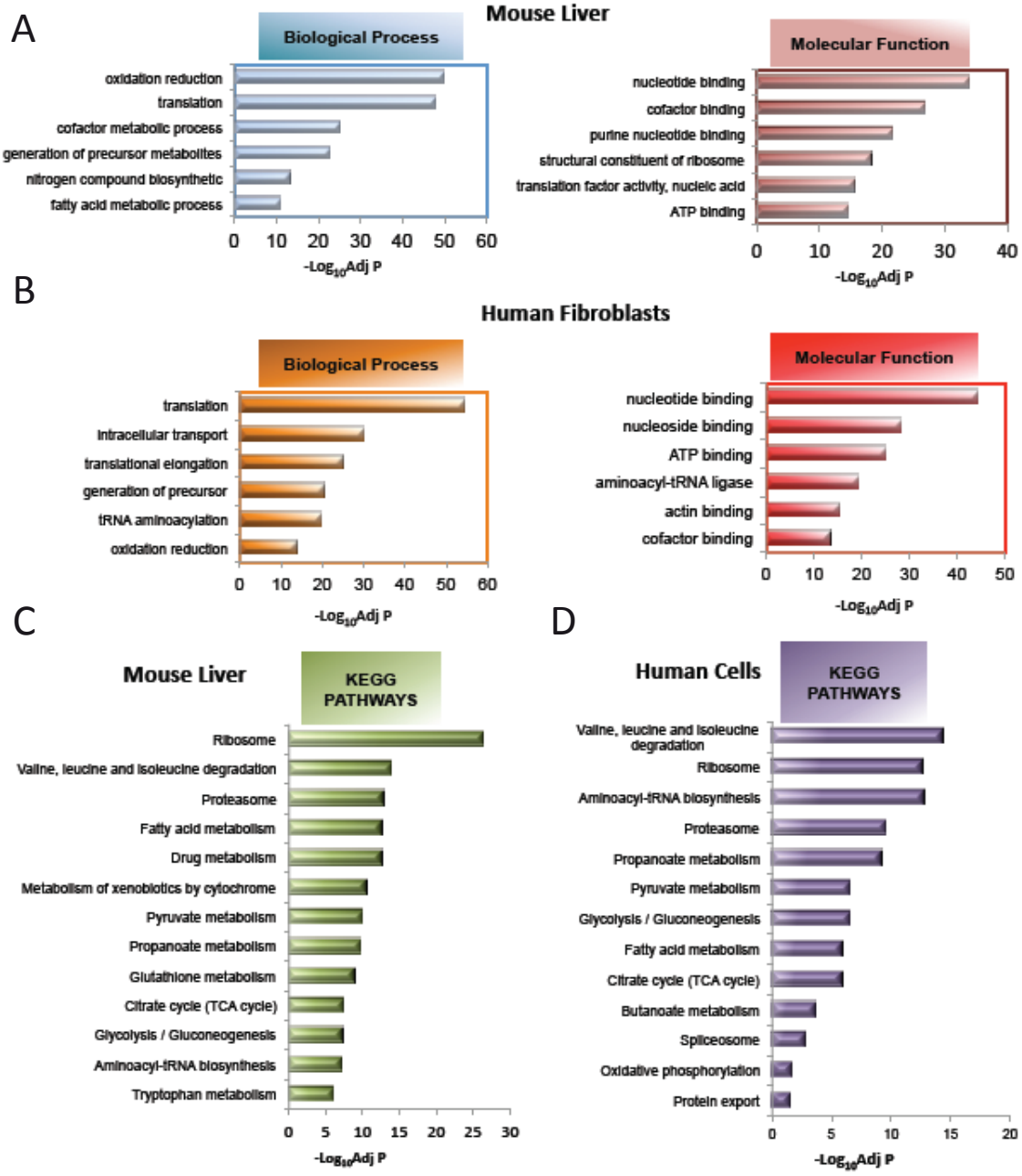

Figure S3 (Related to Figure 5). Pathway analysis of lysine malonylation proteins. (A) and (B) Representative Gene Ontology annotations of Kmal sites for biological process (left) and molecular function (right) in mouse liver (A) and in human fibroblasts (B). (C) and (D), KEGG pathway analysis for lysine malonylated proteins in mouse liver (C) and in human fibroblasts (D).

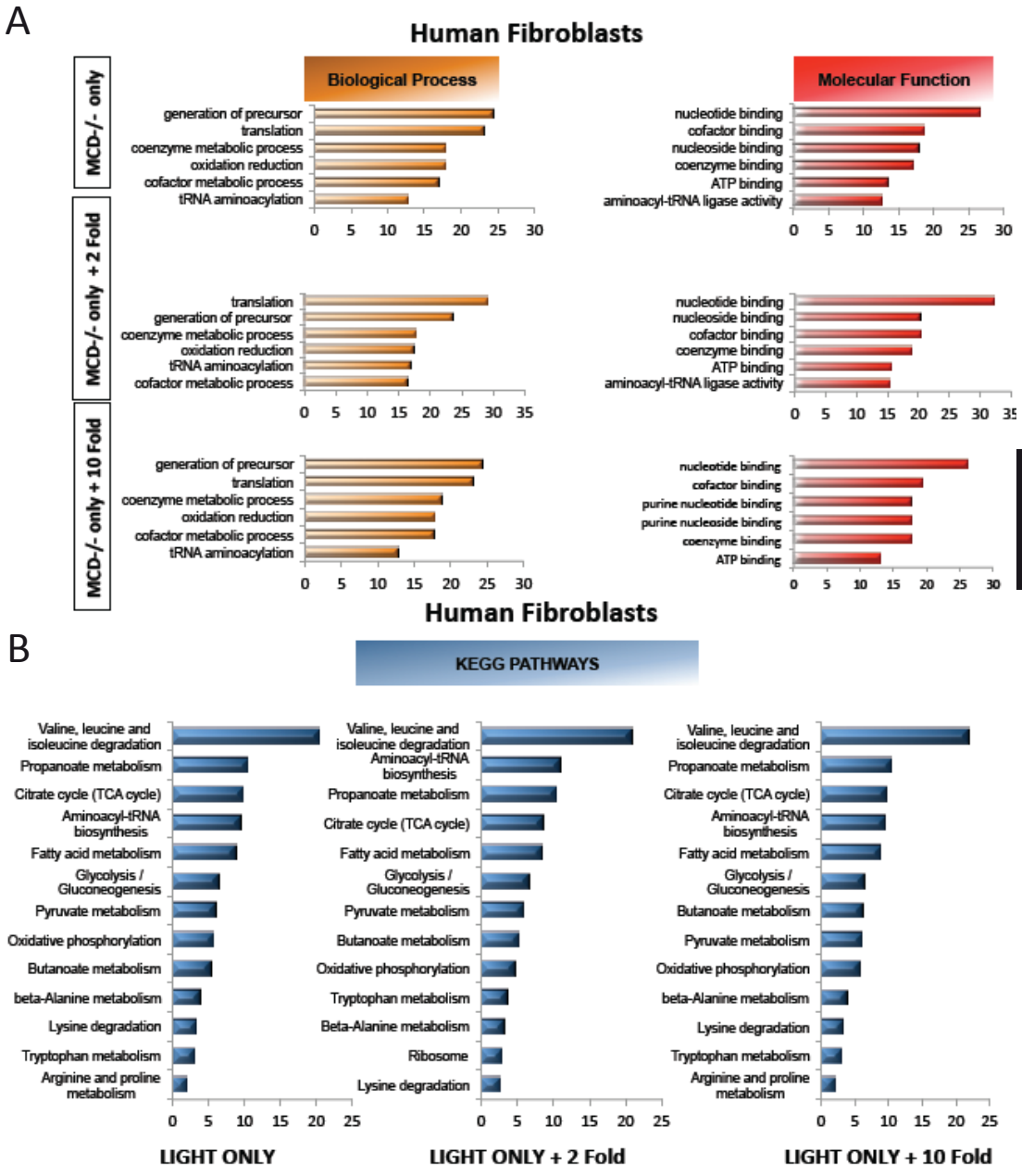

Figure S4 (Related to Figure 5). (A) Representative Gene Ontology annotations of Kmal substrates for biological process (left) and molecular function (right). Top row to bottom: Light-only (MCD-/- only) Kmal substrates, MCD-/- only and 2 fold changed Kmal substrates combined, MCD-/- only and 10 fold changed Kmal substrates combined. (B) Representative KEGG pathway enrichment analysis of Kmal substrates. Left to right: MCD-/- only Kmal substrates, MCD-/- only and 2 fold changed Kmal substrates combined, MCD-/- only and 10 fold changed Kmal substrates combined.

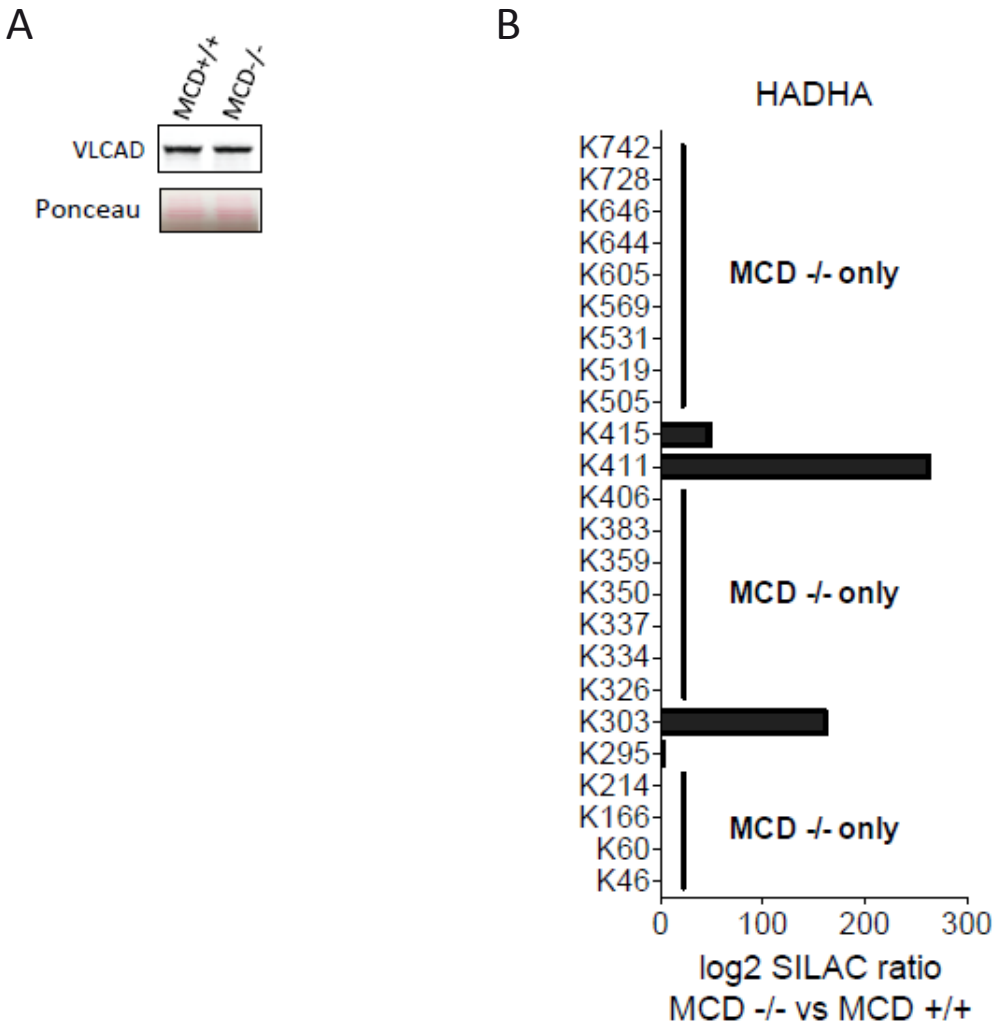

Figure S5 (Related to Figure 7). (A) Western blot analysis of VLCAD levels in $MCD^{+/+}$ and $MCD^{-/-}$ fibroblasts. Cell lysates of each cell line blotted with α-VLCAD antibody and stained with ponceau for loading control. (B) The "Heavy"/"Light" ratios of lysine malonylation sites of HADHA. Determined by quantitative proteomics between $MCD^{+/+}$ and $MCD^{-/-}$ fibroblast cells, respectively.